PM

Hexamethylenetetramine Supporting Halogen Porous Structures

MASTER PROJECT

Goulielmina Anyfanti
MASTER IN NANOCHEMISTRY AND NANOMATERIALS

UNIVERSIDADE da MADEIRA
A Nossa Universidade
www.uma.pt

October | 2017

Hexamethylenetetramine Supporting Halogen Porous Structures

MASTER PROJECT

Goulielmina Anyfanti
MASTER IN NANOCHEMISTRY AND NANOMATERIALS

SUPERVISOR
Kari Rissanen

CO-SUPERVISOR
João Manuel Cunha Rodrigues

Hexamethylenetetramine supporting halogen porous structures

Dissertation submitted to the University of Madeira in fulfilment of the requirements for the degree of Master in Nanochemistry and Nanomaterials

by Goulielmina Anyfanti

Work developed under the supervision of

Professor Kari Rissanen and

co-supervised by Professor João Manuel Cunha Rodrigues

Jyväskylä University, Department of Chemistry, Finland

Faculdade de Ciências Exatas e de Engenharia,

Centro de Química da Madeira,

Campus Universitário de Panteada,

Funchal – Portugal

October 2017

‘’The important thing is to never stop questioning.”

-Albert Einstein.

Declaration

I hereby declare that this thesis is the result of my own work, is original and was written by me. I also declare that its production and publication by Madeira University will not break any third party rights and that I have not previously (in its entirety or in part) submitted it elsewhere for obtaining any qualification or degree. Furthermore, I certify that all the sources of information used in the thesis were properly cited.

Funchal, 11th of October 2017

Dedication

To my two Sisters, my Parents, my Uncle and my friend Francesca for their unconditional love and support.

Acknowledgments

I want to thank all the institutions and researchers that provided support for the development of this thesis.

I also want to thank my supervisor Professor Kari Rissanen and Dr. Rakesh Puttreddy for their help and patience during this one year of the master project at Jyväskylä University, Finland.

Secondly but equally important, I want to express all my gratitude to my co-Supervisor, Professor João Rodrigues and Master Professors Helena Tomás, Pedro Pires and José Câmara for their help, for the immense knowledge provided and the immeasurable motivation that feeds my curiosity.

I want to thank the Department of Chemistry of Jyväskylä University for the equipment and the reagents provided and all its members that helped during my journey in Jyväskylä.

I also express my gratitude to the Madeira Chemistry Research Centre (CQM) for providing all the reagents and equipment during the development of several projects in the two years of Master (Project PEst-OE/QUI/UI0674/2013, CQM, Portuguese Government funds), and to ARDITI-Agência Regional para o Desenvolvimento da Investigação Tecnologia e Inovação through the project M1420-01-0145-FEDER-000005- Centro de Química da Madeira-CQM^{+} (Madeira 14-20).

I want to thank its members for their patience in teaching me and show me all the proper techniques of professional researchers.

I want to deeply thank for helping me in all the difficulties my Master Degree Portuguese colleagues, Natacha Antunes, Ivo Martins and Gina Tavares.

I am thanking all the Professors and Researchers that make the master of Nanochemistry and Nanomaterials a wonderful reality in the incredible island of Madeira.

I want to thank my parents, my uncle, my friends Francesca and Pedro for the support they gave me.

Finally and most important, I want to express all my gratitude and deepest love for my beautiful sisters Maria and Eleni.

Abstract

The increasing spread of nanotechnology has led to the design of new materials that represent a potential solution for several issues such as gas storage and gas separation, shape/size selective catalysis, drug storage and delivery. Among those materials, nanoporous structures have gradually aroused the attention of the scientific community. This interest is witnessed by the increasing number of publications about novel porous materials constructed from the assembly of molecular building blocks such as metal-organic frameworks. The most recent examples are supramolecular porous frameworks. These architectures are built up through traditional noncovalent interactions such as hydrogen bonds, π-π interactions. Most recent discoveries have found a novel type of bond that involves the participation of a halogen atom. This type of interaction assumes the name of halogen bond and is highly directional and hydrophobic. These features can be exploited for the design of defined structures.

The present work is focused on the description of several halogen organic frameworks among which some of them present robust porous architectures. The structures were obtained by combining the tetrafunctional XB acceptor hexamethylenetetramine with different halogen bond donors.

The work is divided into three parts. The literature part gives a background about nanoporous materials and their evolution with a section dedicated to the description of the halogen bond. The experimental section describes the methods used to obtain the supramolecular architectures. The final part discusses the structures and the noncovalent interactions that have driven their assembly.

Keywords: Porosity; X-rays; Halogen bonds; Hydrogen bonds.

Resumo

O contínuo avanço da nanotecnologia potenciou o desenvolvimento de novos materiais que apresentam soluções para variadas problemáticas, das quais são exemplos o armazenamento de gases e sua separação, a catálise seletiva e o desenvolvimento e entrega de fármacos. Devido às suas propriedades, os materiais nanoporosos estão a ganhar destaque, o que levou a um aumento do número de publicações ao longo dos últimos anos, sendo um dos exemplos mais recentes as estruturas supramoleculares porosas. Estas arquiteturas são construídas através de interações não covalentes, como as ligações de hidrogénio e interações π-π. Descobertas mais recentes evidenciam um novo tipo de interação que envolve a participação de um átomo de halogénio, a qual assume o nome de "ponte de halogénio" e é altamente direcional e hidrofóbica.

O presente trabalho teve como objetivo a síntese e caracterização de uma série de *halogen organic frameworks*, resultantes da combinação entre um aceitador hexametilenotetramina e diferentes dadores de halogénio.

O trabalho encontra-se dividido em três partes. A revisão bibliográfica transmite informações básicas acerca dos materiais nanoporosos e a sua evolução, bem como o princípio por detrás da "ponte de halogénio". Por sua vez, a parte experimental descreve a metodologia utilizada para obtenção das estruturas supramoleculares em estudo. Por fim, a terceira secção incide sobre a discussão acerca das referidas estruturas e respetivas interações não covalentes que levam à sua construção.

Palavras-chave: Porosidade; Raios X; Ponte de Halogénio; Ponte de Hidrogénio.

Content

Annexes

List of Figures

Part 1. Introduction

Part 3. Results and discussion

List of Tables

Part 1. Introduction

Part 2. Experimental section

Part 3. Results and discussion

List of acronyms, abbreviations, and symbols

Å – Ångström

a, b, c – Unit cell axes

BDC – 1,4-Benzodicarboxylic

Cu-BTC – Copper-Benzotricarboxylic Acid

DBH – 1,3-Dibromohydantoin

DCM – Dichloromethane

DFT – Density Functional Theory

d_{N---Br} – Distance between nitrogen and bromine atoms

d_{N---I} – Distance between nitrogen and iodine atoms

DMF – Dimethylformamide

HMTA – Hexamethylenetetramine

HOZ – Hierarchically organized zeolite

HB – Hydrogen bond

H_2BDC – Terephthalic Acid

IUPAC – International Union of Pure and Applied Chemistry

MOF – Metal-organic framework

h, k, l – Miller Indices

NBS – N-bromosuccinimide

NCS – N-chlorosuccinimide

NIS – N-iodosuccinimide

PFC-HC – Perfluorocarbon – halocarbon

SBU – Secondary building unit

SEM – Scanning Electron Microscopy

TEM – Transmission Electron Microscopy

TPAOH – Tetrapropylenammonium hydroxide

vdW – van der Waals

XB – Halogen bond

ZSM-5 – Zeolite Socony Mobil-5

Z – Number of formula units per unit cell

α, β, γ – Unit cell angles

μ - Linear absorption coefficient

ρ – Density

1. Introduction

1. 1 Nanoporous materials - an overview

Materials consisting of nanostructures are abundant in nature. Examples are proteins, DNA, or even thinking on nanoparticles used from millenniums to colour glasses and ceramics. The real novelty of the last four decades relies on the increase of the ability to fabricate nanostructures and nanosystems with a great degree of control and using a diversity of techniques, accompanied by a similar enhancement in the ability to characterize structures and systems at the nanoscale.[1] Nowadays, nanomaterials are designed tailoring their properties and functionalities. Anyway, what is exactly nanotechnology, nanoscience and all those fields that encompass the nano-world? To answer this question it would be appropriate to borrow the definition gave by Professor Roald Hoffmann - the Chemistry Nobel Laureate in 1981: *"Nanotechnology is the way of ingeniously controlling the building of small and large structures, with intricate properties; it is the way of the future, with incidentally, environmental benignness built in by design*''.[1]

Its rise has started since the quantum physics laws prevailed to the classical ones that perfectly fit the description of macroscale phenomena. By decreasing the scale from macro to nano, the properties of the matter change as the energy is discretised and its dependence on surface to volume ratio surprisingly increases.

Certainly, several types of nanostructures materials exist. Among these, nanoporous ones represent one important type of nanostructures materials. They consist of a regular organic or inorganic framework supporting a regular, porous structure.[1] They possess specific surface, structural and bulk properties that make them applicable in many fields such as ion exchange, separation, catalysis, sensor, and purification. Their pore size in the range of nm makes them suitable for the absorption and the interaction with atoms.

Based on the pore size, it is possible to classify the nanoporous materials in three categories:

1) Microporous – materials have pore diameters of less than 2 nm.[2]

2) Mesoporous – materials have pore diameters between 2 nm and 50 nm.

3) Macroporous – materials have pore diameters of greater than 50 nm.[3]

In the present context, the attention is turned to those nanoporous solids possessing a pore size of similar magnitude or only slightly larger than common gas molecules.

More specifically, the next paragraphs give an overview of the different nanoporous materials following the timeline of their development. Afterwards, the attention is focused on the organic frameworks spacing from the metal organic ones, the so-called MOFs until the recent halogen organic frameworks (XOFs) which represent the main object of this study.

1. 2.1 The first example of nanoporous materials: Zeolites

Zeolite are natural mineral discovered in 1756 by the Swedish mineralogist Axel Fredrik Cronstedt.[4] He observed that after heating this mineral, steams of water were produced. This observation inspired the mineralogist to call these materials zeolites, from the Greek ζέω (zéō), meaning "to boil" and λίθος (líthos), meaning "stone".

Zeolites are crystalline aluminosilicates of group IA and group IIA elements, such as sodium, potassium, magnesium, and calcium[5] with microporous structures of usually below 1.0 nm in diameter.[6] They have the chemical formula $M_{2/n}OAl_2O_3{\cdot}xSiO_2{\cdot}yH_2O$, where the charge-balancing non-framework cation M has valence n, x is 2.0 or more, and y is the number of moles of water in the voids.[4] Therefore, they are solids with a relatively open, three-dimensional crystal structure built from the elements aluminum, oxygen, and silicon, with alkali or alkaline metals plus water molecules trapped in the gaps among them.[7] Aluminium and silicon atoms form a three-dimensional structure of AlO_4 and SiO_4 tetrahedra linked together through an oxygen atom. If the SiO_4 results already charge balanced, AlO_4 is negatively charged and, thus, is balanced by a cation, M (Fig. 1). The content ratio of Si/Al modifies the properties of porous zeolite. More specifically, a higher content of aluminium increases the acidity of the porous structure; oppositely, a higher amount of silica makes the zeolitic environment more basic. Depending on the application, the content ratio varies, and several zeolites with different properties are obtained.

Important characteristics of zeolites are high boiling points (over 1000°C), resistance to high temperatures, high-pressure resistance and difficulties to dissolve in water and organic solvents. Even if all these properties are enough for making them good candidates for many applications, they are more notable for their open, cage-like, framework structure. In fact, they present a high surface to volume ratio, and, consequently, a huge porous volume. This peculiar feature led to their use in separation, filtration, adsorption, and catalysis. Several types of natural zeolites exist such as chabazite, erionite, mordenite, and clinoptilolite. Anyway, the random size porous distribution makes natural zeolites not suitable for many applications. Differently, manufactured zeolites present a precise dimension and pore size distribution.

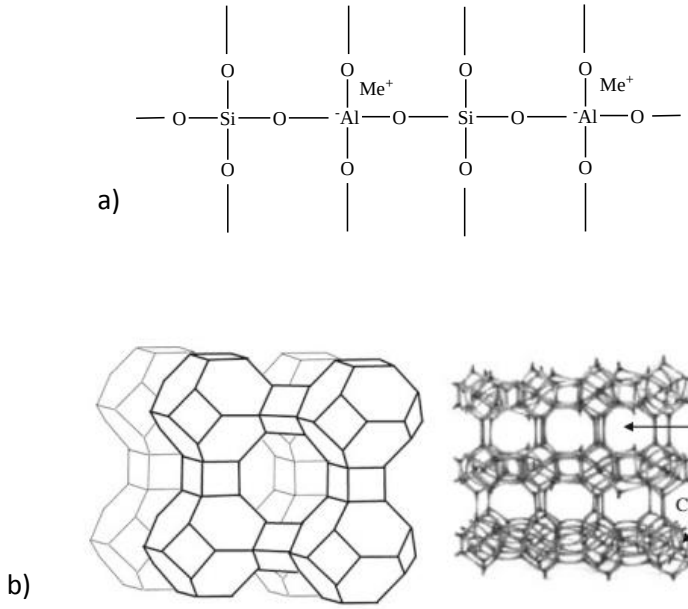

Figure 1 - a) Schematic structure of Zeolite and b) 3D network of silica and alumina in zeolite.[8]

One of the most famous examples of synthetic zeolite applied for petroleum cracking process is Zeolite Socony Mobil - 5 (ZSM-5) with the chemical formula $Na_nAl_nSi_{96}–nO_{192}·16H_2O$ (0<n<27). The Mobil Oil Company patented it in 1972 for the petroleum industry. It possesses a pentasil unit characterised by eight five-membered rings with the Al and Si atoms on the vertices (Fig. 2). Each

unit is interconnected with the other through oxygen atoms forming, thus, corrugated sheets with 10-ring holes

Figure 2 - Pentasil unit of ZSM-5.[9]

Robert J. Argauer and George R. Landolt performed the first synthesis of ZSM-5 in 1969.[10,11] Their method consisted of a mixture of three solutions. One solution corresponded to the source of aluminium, sodium and hydroxide ions. The second one contained tetrapropylammonium cation as a templating agent. The third solution was the source of the other building block of zeolites, silica. The mixture of the three solutions led to the supersaturation point of the tetrapropylammonium ZSM-5. After heating and recrystallization, the solid ZSM-5 were obtained.

Even though the proposed method was easy to perform, it presented some drawbacks such as the use of toxic and readily inflammable ammines. The subsequent years witnessed other procedures to synthetize ZSM-5 without involving dangerous compounds.[12,13,14]

The next paragraph deals with the current role of zeolites in the industrial field. Mainly the catalytic activity of them is presented showing advanced zeolitic structures such as nanocrystal zeolites and hierarchical zeolites.

1. 2.2 Zeolites current industrial application

Zeolites can be divided into two categories, natural and synthetic zeolites. Even if the first ones were discovered almost 250 years ago, their use for industrial applications came just when artificial zeolites were synthesized. Figure 3 presents the milestone in the history of Zeolites.[15]

Figure 3 - Milestone in the history of Zeolites.[15]

The major applications for synthetic zeolites are in ion exchange (detergents), adsorbents/desiccants and catalysis.[16] They are also defined as molecular sieves to stress their ability on allowing small molecules to enter the nanopores instead of the biggest ones.

For all those characteristics, they are intensively used, as already mentioned, in catalytic activities. Catalyst materials are important for decreasing the activation energy barrier in a reaction. Their application allows lower reaction temperatures to be used during the process. Zeolitic catalysts are mainly employed in pharmaceutical drug production and in the petrochemical industry as catalytic crackers to break large hydrocarbon molecules into gasoline, diesel, kerosene, waxes and more petroleum by-products. Their catalytic activity is due to their porous structure. The several atoms and molecules once enter zeolites remain trapped into the tiny cavities and, thus, reactions readily take place.

On the other hand, the narrow micropores of zeolites also imply access and diffusion limitations[17] of the reagents/products throughout the crystal. This threat can be solved either decreasing the crystal size, creating nanocrystals zeolites with a size typically smaller than 0.5 μm,[18] or through the synthesis of hierarchical zeolites.[17] The reduction of the size of a particle from the micrometer to the nanometer scale leads to substantial changes in the properties of zeolites,

and consequently of their performance in catalysis among other properties. The surface to volume ratio increases by the decrease of materials dimension and zeolite nanoparticles acquire large external surface areas and high surface activity. In addition, smaller zeolite crystals have reduced diffusion path lengths relative to conventional micrometer-sized zeolites.[19] Tuel *et al.*[18] reported an efficient method to synthesized hollow zeolites nanocrystals (ZSM-5) with a controllable wall thickness and chemical composition. The formation of holes in the crystals involves both partial dissolution and re-crystallization of the zeolite in the presence of a base and organic molecules. More specifically, synthesized calcined silicalite-1 nanocrystals, with the composition $Si_{96}O_{19}2F_4(TPA)_4$ were immersed in a solution of tetrapropylenammonium hydroxide (TPAOH) with water and different contents of aluminium, introduced as aluminium nitrate $Al(NO_3)_3$, to obtain Si/Al molar ratios between 25 and 100. The nanocrystals were obtained after periods of static heating at 170°C. Figure 4 shows TEM and SEM pictures of the nanocrystals obtained by simple crystallization of silicalite-1 zeolites and after its dilution in TPAOH in the presence of aluminium, getting ZSM-5. The ‘‘nanoboxes” possess very regular zeolitic walls, with a thickness in the 20–40 nm range. In SEM pictures is evident that internal voids never communicate with the outside via large pores, and that all zeolite nanoboxes look perfectly closed at the resolution of the pictures. The presence of aluminium slightly influences the intracrystalline pore size and shape as possible to observe from TEM images. Values in Table 1 show that the volume is similar for hollow silicalite-1 and ZSM-5 zeolites obtained after dissolution of silicalite-1 in TPAOH solution in the presence of aluminium.

Nanocrystals zeolites have been recognized as a possible solution for the diffusion limitation that such materials present. On the other hand, hierarchical zeolites have provided a new way to avoid diffusion limitation.

A hierarchically organized zeolite (HOZ) is defined as a material that retains the crystalline order and associated functionality of bulk (purely microporous) zeolite, but that also integrates a multilevel pore network.[20] The new porous material is characterized by an interconnection of micro-, meso- and macropores to enhance the molecular transport in the active sites (Fig. 5). The additional porosity levels can be configured either within (intracrystalline) or between

(intercrystalline) the zeolite crystals, effectively shortening the diffusion path inside the micropores in both cases.[20]

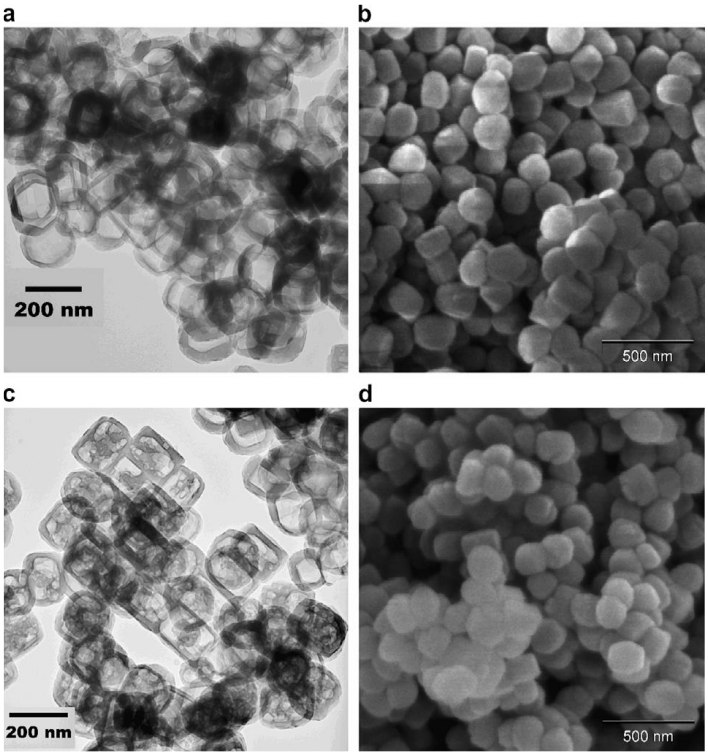

Figure 4 - TEM (a) and SEM (b) pictures of hollow pure-silica zeolite obtained by treating silicalite-1 crystals at 170 °C for 24 h in TPAOH (c) and (d) correspond to TEM and SEM pictures of hollow ZSM-5 obtained in the presence of aluminium.[18]

Table 1 - Textural properties of hollow zeolites.[18]

Sample	Re-crystallization conditions at 170°C	V_{int} (cm^3g^{-1})
Hollow S1	24h	0.12
Hollow ZSM-5	45 min	0.019
	1h30min	0.05
	3h	0.095
	24h	0.11

S1 = silicalite-1

V_{int} = internal volume estimated by the difference calculated between desorption and adsorption branches at $p/p_0 = 0.5$

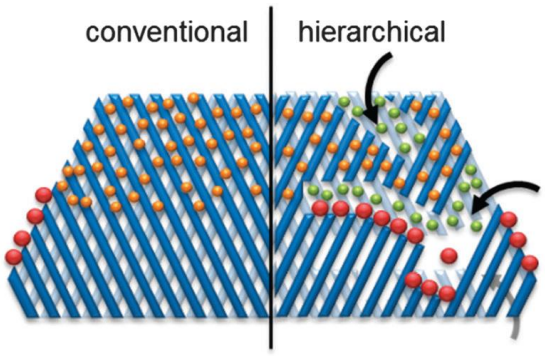

Figure 5 - Schematic representation of access and transport/diffusion limitations in conventional and hierarchical zeolites. The orange spheres represent molecules that suffer from single-file diffusion. The secondary porosity enhances the number of pore mouths to diffuse in and out of, as well as the diffusion properties within the pores (indicated by the green spheres). In the latter case, the introduction of external surface often leads to enhanced selectivity. The red dots represent bulky molecules, which can only react on pore mouths.[17]

Approaches to synthesize HOZs involve either interrupting their crystallization and growth in the synthesis gel (bottom-up) or a post-synthetic removal or rearrangement of the atoms in a bulk zeolite (top-down) (Fig. 6).[20]

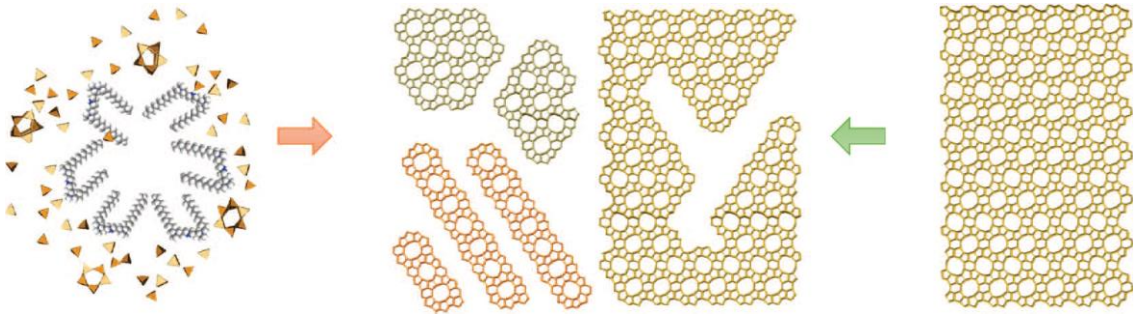

a) Bottom-up *b) Top-down*

Figure 6- a) Bottom-up from gel solution; b) top-down approach for nanoporous zeolites formation.[20]

Nanocrystal zeolites and hierarchical zeolites represent significant advances for the rationalization of zeolite synthesis.[21] However, the prediction of their final crystal structure is not easy as well as their functional tunability.

The progress in coordination chemistry has led to the synthesis of metal-organic frameworks (MOFs), which imply a better prediction of the resulting crystal structure based on the knowledge of the metal clusters and the organic ligands participating in the synthesis.[22]

1. 3.1 Metal Organic framework – An introduction

Generally, the robustness of a framework can be achieved by the combination of rigid organic moieties and inorganic clusters. This attempt has led to the synthesis of the so-called metal-organic frameworks (MOFs) as shown in Figure 7.

They consist of metal units, secondary building units (SBUs), linked with organic moieties using coordination bonds (Fig. 8).[23]

This new category of porous materials did not occupy the main role in the scientific panorama until 1990. Prior to the early 1980s, aluminosilicate zeolites and closely related systems represented the predominant class of open-framework materials with three-dimensional crystalline structures.[24,25,26]

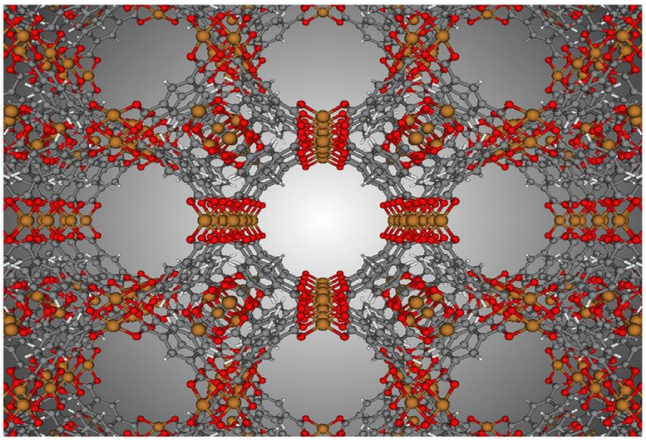

Figure 7- Molecular structure of the metal organic framework called Cu-BTC. The spheres represent atoms, and the sticks show how the atoms are bonded to each other; different colours are used for different elements (orange: copper, red: oxygen, grey: carbon, white: hydrogen).[27]

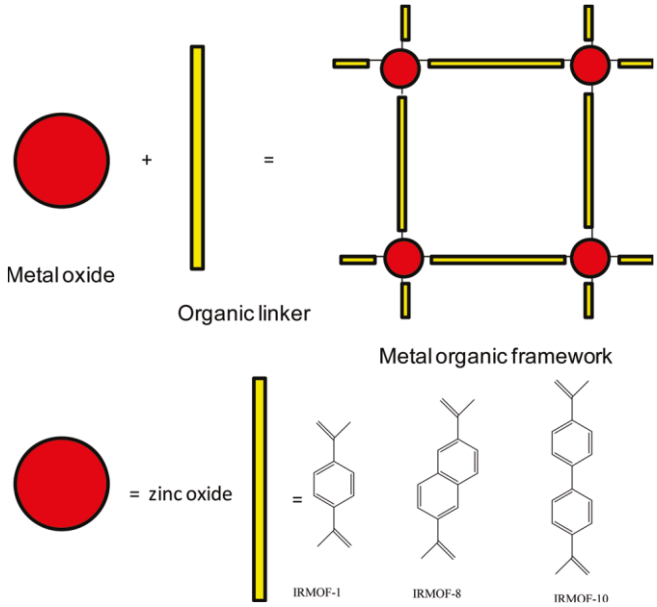

Figure 8- Building blocks of metal-organic frameworks.[28]

Parallel, the coordination chemistry led to the divulgation of the coordination polymers. These consist of metal ions joint together by organic ligands. As mentioned before, the real interest in porous coordination polymers and MOFs started only around 1990.[24] These new structures have a great advantage over the common zeolites: more flexible rational design.[29] Nevertheless, the stability of these hybrid structures was achieved later. Indeed, until the end of the '90, some issues compromised their formation. First of all the final products were poorly crystallized and prevented structure information from being obtained. Then, their thermal stability initially was low, and many structures collapsed in the absence of the guest molecules.[25] The evolution came with the discovery of MOF-5 by Yaghi and co-workers in 1999.[29]

In Robson's paper[30] published in 2008, it is traced the synthetic development of MOFs that led to the formation of a large range of crystalline, microporous, stable solids, possibly using structure-directing agents, with ion-exchange, gas sorption, or catalytic properties.

MOFs have emerged as an extensive class of crystalline materials with ultrahigh porosity (up to 90% free volume) and enormous internal surface areas, extending beyond 6 000 m^2/g.[24] This feature combined with the changeable structure and properties caused by the large choice of both organic and inorganic components, make MOFs good candidates in applications such as clean energy, storage of gases (e.g., hydrogen and methane), adsorbents for separation needs. More

potential applications are catalysis and biomedical imaging. All these positive aspects have seen an increasing interest on MOFs parallel to the development of different chemistry fields:

1) Advances in cluster chemistry.

2) Maturation of organic synthesis pertinent to ligand preparation and post-synthetic modification.

3) Improvement in structure determination, particularly through X-Ray crystallography, and development of hard- and software for evaluation of sorption properties.

4) Interdisciplinary growth of MOF research with its neighbouring fields.

5) The ever-expanding potential in applications.[31]

One more important feature of MOFs is their geometrically well-defined structure. This property further implies that these solids should be crystalline, an important criterion for the precise establishment of structure-property relationships.[32] Nevertheless, this is not the only implication. The knowledge of possible topologies, the functionality of multitopic organic linker molecules, as well as the understanding of typical metal coordination environments, helps to understand and direct the synthesis efforts. As ultrahigh porosity is the feature that made MOFs so famous, the main goal in MOF synthesis is to establish the conditions that lead to a framework, which does not collapse.

Moreover, as they are crystalline solids, a tuneable kinetics of crystallization is of huge importance to guarantee the nucleation and, consequently, the growth of crystals. As nothing is known in details about their crystal growth and nucleation process, a new type of MOF is discovered by the common trial-and-error method.

First of all, the formation of this kind of hybrid frameworks is a consequence of supramolecular chemistry.[30] Thus in the assembly process, two subunits have to be combined, organic ligands and metal precursors.[33] Whereas the organic ligands are supplied directly as a reactant, the SBUs have to be formed in the synthesis process from the metal precursors. What results crucial is the SBUs synthesis that ascertains the MOF assembly process.[29] The advantage to common nanoporous materials such as zeolite is the easiness on tuning their structure and functionality

during synthesis. Moreover, as the subunits of MOFs are the metal coordination centres and the organic linkers, by changing the last ones, it is possible to obtain a wide range of structures that differ from pores 'size, chemical functionalities and affinities for guest molecules.[28,34]

Depending on the different stages of synthesis involved, MOFs are classified as

i) first generation (normal MOFs);

ii) second generation (functionalized MOFs);

iii) third generation (smart MOFs).

First-generation MOFs possess the traditional architecture having an inorganic and organic moiety, second-generation MOFs are subjected to surface modifications through chemical functionalities and, finally, third-generation MOFs contain biomolecules such as cations, drugs, bioactive compounds, toxins and gases within their framework.[35]

MOFs can also differ for the characteristic framework they possess. In this sense, they can be categorized into two groups, rigid and flexible. A permanent porosity and robust pores characterize the first type. The second one is dynamic and responds to external factors such as temperature, pressure or even guest molecules.

The broad range of MOFs published through the years is huge and it results impossible to present all of them. The following text discusses about MOF-5, one of the principal metal-organic frameworks.

1. 3.2 The father of MOFs- MOF-5 and its application

This paragraph is dedicated to the description of MOF-5 developed in 1999 by Yaghi and co-workers.[29]

It is also called IRMOF-1 standing for isoreticular and means a series of MOFs with the same topology, but different size of pores. MOF-5 is a metal-organic framework formed from tetranuclear supertetrahedral cluster consisting of Zn_4O that constitutes the nodes separated by 1,4-benzodicarboxylic (BDC) acid struts.[29] More specifically the structure derived from a simple cubic six-connected net in two stages: first, the nodes (vertices) of the net are replaced by clusters of secondary building units; second, the links (edges) of the net are replaced by finite rods (`struts') of

BDC molecules. The core of the cluster consists of a single O atom bonded to four Zn atoms, forming a regular Zn_4O tetrahedron. Each edge of each Zn tetrahedron is then capped by a CO_2 group to form a $Zn_4(O)(CO_2)_6$ cluster. Figure 9b shows the sphere that represents the pore size that can be used for gas storage.

The structure was obtained by a solvothermal method in mild conditions. That means a solution of the metal precursor (Zinc II Nitrate) in trimethylamine was mixed with a solution of H_2BDC in N,N'-dimethylformamide (DMF)/chlorobenzene. The solid-state ^{13}C NMR analysis of the obtained colourless crystal blocks confirmed the inclusion of DMF and chlorobenzene molecules in the voids. This stability was confirmed after heating up to 300°C for 24h the desolvated crystals. Incredibly, both the morphology and the crystallinity remained unaltered as the single crystal X-ray analysis confirmed.

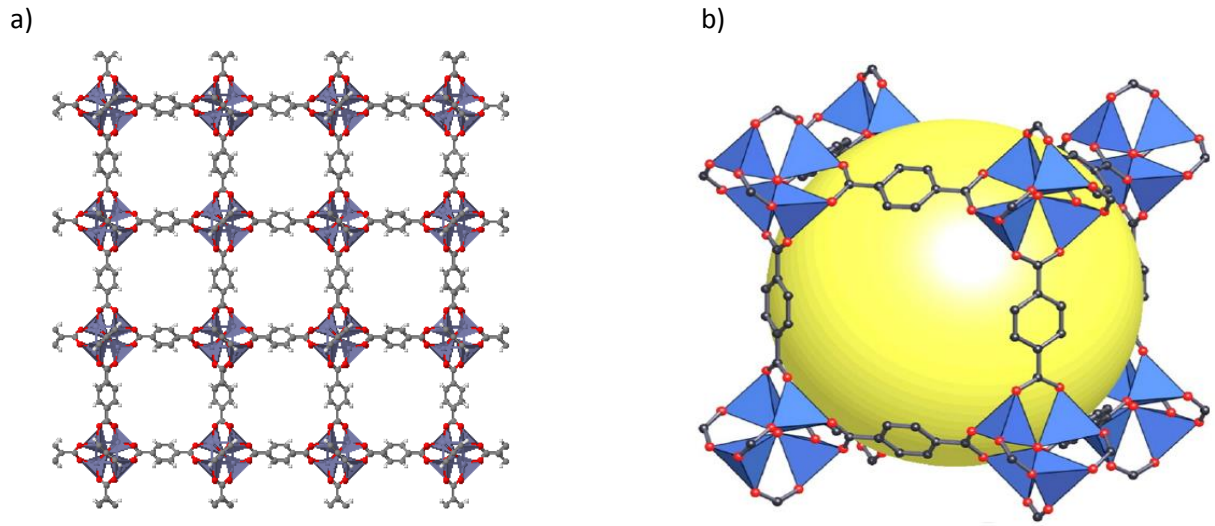

Figure 9 - MOF-5 crystal relative packing[36] (a) and the void dimension (b).[37]

Without considering the guest molecules in the voids, the 80% of the cell volume stayed unoccupied. This characteristic indicates the high surface to volume ratio (surface/volume) reached.

This incredible success derived from the commitment between organic and inorganic chemistry and traced the starting point of the research and development of several MOFs.

1. 4.1 An introduction to halogen bond

Porous materials constructed from molecular building blocks, such as MOFs, have received continuous interest for not only their diverse and designable structures but also for their dynamic behaviors under external stimuli.[38] Supramolecular organic frameworks that are acquiring more and more attention due to their easy synthesis represent a relatively new class of porous materials. Among the wide range of these molecular materials, the last decade has seen the rise of the halogen organic frameworks. As the name suggests, the structures are built up on motifs that self-organize through the halogen bond recognition. Indeed, as halogen atoms in organic compounds can typically be found at the periphery of molecules, they are ideally positioned to be involved in intermolecular interactions.[39] This noncovalent interaction is less familiar than hydrogen bond but it is similar to it in several respects.[40]

It results, thus, important to clarify what halogen bond is. Any noncovalent intermolecular arrangement R – X···Y, where X is the halogen atom, is included in the definition[41] of halogen bond (Fig. 10). This peculiar interaction exists when an electron density transfer occurs from the electron donor site, Lewis base, to the halogen atom, Lewis acid.[42] The attractive nature of the interaction results in intermolecular distances shorter than the sum of the van der Waals (vdW) radii of the involved atoms. The characteristics of these noncovalent interactions depend on the nature of the interacting partners that determine the final architecture of a supramolecular system. The nature of the halogen bond donors and acceptors influence the final architecture in a supramolecular system. Molecules possessing nitrogen, oxygen and sulphur atoms are good XB acceptors.

On the other hand, the XB donors are characterized by a halogen atom high polarizable and less electronegative. They are involved in a covalent bond with an atom quite electronegative, such as nitrogen, which withdraws the electron density intensifying the electropositive area on the halogen alongside the bond. However, generally the halogen bond donor ability decreases in the order I > Br > Cl.[43] Fluorine is not even considered because of its weakness in forming XBs.

Figure 10 - Schematic representation of halogen bonding interaction.[44]

Halogen bond occurs due to an anisotropic distribution of the electron density around the halogen atom. This anisotropic character determines the formation of a region of positive electrostatic potential on the outermost portion of some covalently bound halogen atoms.[45] The electron density is represented by an ellipsoid elongated in the direction of the bonding axis, a feature called polar flattening.[46] Consequently, the XB is a high directional type of bond. Regarding crystal engineering, this feature is exploited to tailor the design of new porous materials useful for gas storage and for the adsorption of volatile organic compounds,[47] drug delivery systems,[48] fuel cells, ion exchange and CO_2 capture.

Halogen bonding is mainly explored in co-crystals between iodine perfluorocarbons and nitrogen-containing compounds,[46] but the discovery of porous molecular crystals from a mixture of hexamethylenetetramine (HMTA) and N-iodosuccinimide (NIS) has broadened the non-fluorine based halogen bond donors to N-haloimides.[49]

The present project deals with the design and formation of crystals of which motif is built up through XBs. For this reason, it is of great importance to clarify, as far as possible, some main features of this noncovalent interaction starting from the historical background that led to the discovery of this new class of supramolecular bonds.

1. 4.2 A historical background

The history of the halogen bonding (XB) is approximately 200 years old as the $I_2\cdots NH_3$ adduct, probably the first halogen-bonded system ever prepared, was synthesized in Gay-Lussac's laboratory by Colin as early as 1813 (Fig. 11).[50] Colin reported that when dry gaseous ammonia and dry iodine are reacted, a liquid with a somewhat metallic luster is produced. Fifty years later, Guthrie obtained the same liquid in pure form by adding powdered iodine to aqueous ammonia and proposing the compound structure as $I_2\cdots NH_3$.

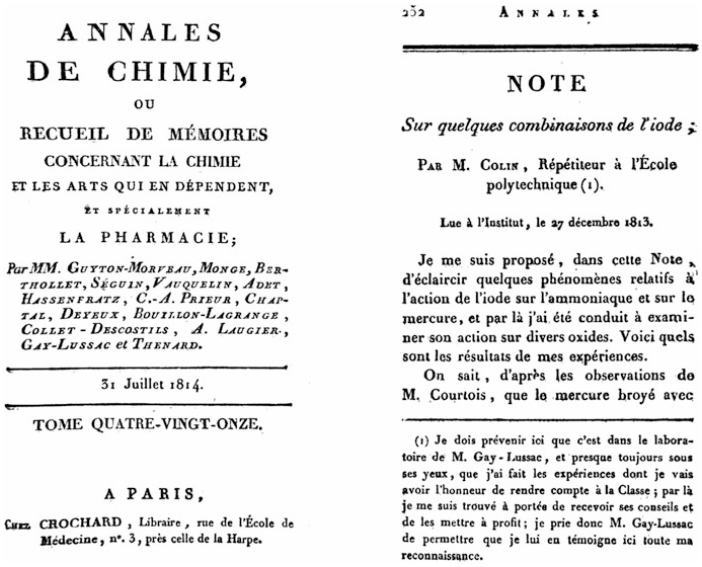

ANNALES
DE CHIMIE,
OU
RECUEIL DE MÉMOIRES
CONCERNANT LA CHIMIE
ET LES ARTS QUI EN DÉPENDENT,
ET SPÉCIALEMENT
LA PHARMACIE;

Par MM. Guyton-Morveau, Monge, Berthollet, Séguin, Vauquelin, Adet, Hassenfratz, C.-A. Prieur, Chaptal, Deyeux, Bouillon-Lagrange, Collet-Descostils, A. Laugier, Gay-Lussac et Thenard.

31 Juillet 1814.

TOME QUATRE-VINGT-ONZE.

A PARIS,

Chez CROCHARD, Libraire, rue de l'École de Médecine, n°. 3, près celle de la Harpe.

252 ANNALES

NOTE

Sur quelques combinaisons de l'iode ;

Par M. Colin, Répétiteur à l'École polytechnique (1).

Lue à l'Institut, le 27 décembre 1813.

Je me suis proposé, dans cette Note, d'éclaircir quelques phénomènes relatifs à l'action de l'iode sur l'ammoniaque et sur le mercure, et par là j'ai été conduit à examiner son action sur divers oxides. Voici quels sont les résultats de mes expériences.

On sait, d'après les observations de M. Courtois, que le mercure broyé avec

(1) Je dois prévenir ici que c'est dans le laboratoire de M. Gay-Lussac, et presque toujours sous ses yeux, que j'ai fait les expériences dont je vais avoir l'honneur de rendre compte à la Classe ; par là je me suis trouvé à portée de recevoir ses conseils et de les mettre à profit ; je prie donc M. Gay-Lussac de permettre que je lui en témoigne ici toute ma reconnaissance.

Figure 11 - Frontispiece of the volume (left) and the first page of the paper (right) where Colin was reporting his experiments on the reaction of diiodine with ammonia.[50]

Just after 1950, the chemistry community started to figure out the existence of a strong electrophilic nature of halogens. Until that time, the recognition of electrophilic halogens as responsible for the formation of relatively strong and directional interactions in the solid, liquid, and gas phases was denied by the entire community.[50] In 1954 Hassel *et al.*[51] described the solid-state structure of the $Br_2\cdots O(CH_2CH_2)2O$ system (Fig. 12, top). In 1958 and 1959 two more structures were reported, $Br_2\cdots C_6H_6$ (Fig. 12, bottom) and $Cl_2\cdots C_6H_6$ adducts,[50] showing that π-systems work

as donors of electron density to the electrophilic halogens even in the solid state. The use of ‘’halogen bond’’ to identify this interaction progressively became less and less occasional, and an exponential growth occurred in the last 20 years in parallel with the comprehensive process of unification of all phenomena related to interactions originated by electrophilic halogens.

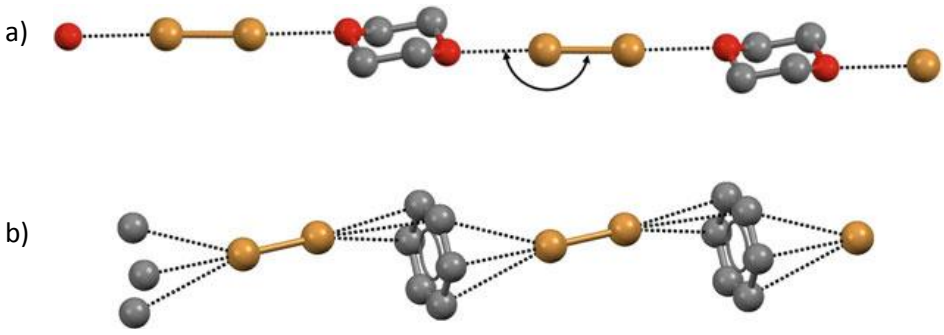

Figure 12 - Ball and stick representation of infinite chains formed by dibromine with 1,4-dioxane (a) and benzene (b). XB are black dashed lines. Color code: gray, carbon; red, oxygen; brown, bromine. Hydrogen atoms have been omitted for clarity.[50]

1. 4.3 A physical study of halogen bonds: the σ-hole

The formation of chemical bonds, wherever they may fall on the continuum between covalent and noncovalent, involves a balancing of attractive and repulsive forces within the system. Once at equilibrium, the forces felt by the nucleus are zero. These forces have a nature purely Coulombic. In a molecule, nuclei with electrons exercise a potential, which can be defined as:

$$V(r) = \Sigma \, (Z_A / |R_A - r|) - \int (\rho(r')dr' / |r' - r|) \qquad \text{eq.1}$$

Where Z_A is the charge on nucleus A, located at R_A. The denominators are the distances from each nucleus A and each unit of electronic charge ρ(r ’)dr from the point of interest r.[52]

When there is no perturbing effect, the electron density ρ(r) is static, and the corresponding potential is defined as electrostatic potential. The electrostatic potential is a property of fundamental significance[53] and it is useful in predicting noncovalent interactions areas with positive

V(r) of a molecule that attracts areas of negative V(r) of another molecule. Generally, the literature refers to surface $V_S(r)$ as the potential is computed on the surface of the molecule. The latter is defined by the 0.001 au contour of its ρ(r).[54] When the electrostatic potential is positive is indicated as $V_{s,max}$ and where is negative it is labeled $V_{s,min}$.

Once the concept of electrostatic potential is clarified the comprehension of the σ-hole, a basic concept in halogen bonds, results easier.

Considering a simple free halogen atom, it presents an overall electron density distribution with a spherical symmetry and a positive potential.[55] When the same atom forms a covalent bond with an atom B, the spherical symmetry is disrupted, and the electron density undergoes to an anisotropic distribution. More specifically the electron density would be less along the extension of the bond than on the lateral sides. The area with less electron density is called “σ-hole”. The name is due to the electron-deficient outer portion of the half-filled bonding orbital.[56] The presence of the σ-hole causes the electrostatic potential $V_S(r)$ on the surface of the covalent bond to assume different signs. In fact, what is often found is that $V_S(r)$ is positive in the σ-hole region, which has the lesser electronic density, and it is negative on the lateral sides, which possess greater electronic densities.[52] Figure 13 shows the computational calculation of the $V_s(r)$, performed with DFT methods, in chlorine when forming the covalent bond in Cl-OH. As it is possible to observe, the positive potential indicated with the red color corresponds to the σ-hole along the O–Cl bond.

In general, the more polarizable the halogen atom and the more electron attracting the skeleton of the molecule, the more positive is the halogen σ-hole. Thus, the XB-donor ability is greater for the heavier and more polarizable halogens. It increases according to the order Cl<Br<I. The fluorine atom, even if it belongs to the VII group of the periodic table, it is so electronegative that it is not common to behave as an XB donor as it does not possess an extensive σ-hole. Just in cases where the electron donor is highly strong, fluorine shows a σ-hole interaction.[57] The presence of a σ-hole on many covalently bound halogen atoms gives rise to attractive noncovalent interactions, both inter- and intramolecular, with negative sites such as the lone pairs of Lewis bases, π electrons, anions, etc.[55]

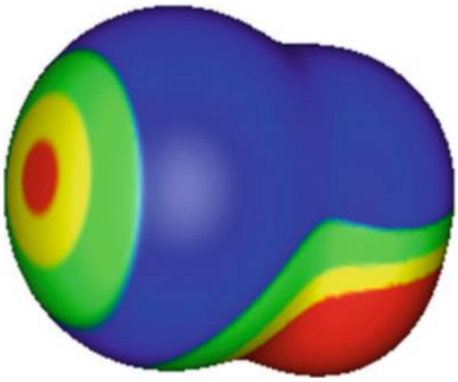

Figure 13 – DFT calculations of the electrostatic potential on the molecular surface of Cl-OH. Chlorine is on the left. Color ranges, in volts: red, greater than 0.87; yellow, from 0.87 to 0.43; green, from 0.43 to 0; blue, less than 0 (negative). The most positive potential on the chlorine surface (red) has a $V_{S,max}$ of 0.99 V, and corresponds to a σ-hole on the extension of the O–Cl bond. Note also the positive region associated with the hydrogen (lower right); the $V_{S,max}$ is 2.51 V.[55]

These interactions result high directional. Indeed, if a halogen atom X is covalently bound with an atom R, the resulting interaction with either a nucleophilic or an electrophilic site will be along the covalent bond (linear) in the first case, and on the lateral side in the second case (Fig. 14).

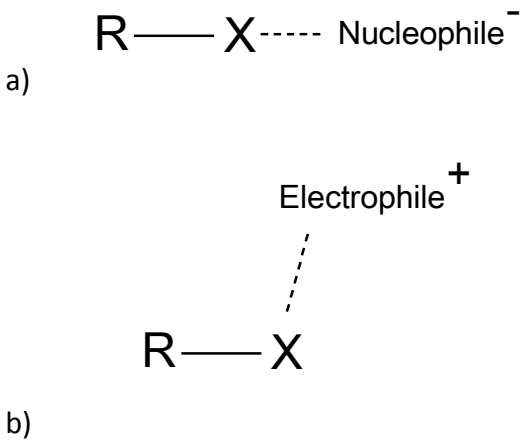

Figure 14 - Schematic representation of the directional interaction between covalently bound halogen atoms with nucleophilic (a) and electrophilic (b) moieties.

The more linear the X···Nucleophile bond is, the stronger the interaction results. This means that the distance between the two atoms is shorter. Therefore, the length and the linearity of the bond indicate how strong the interaction is.

Now the question is what is the real, physical nature of this interaction? What is the nature, so, of the σ-holes? Through the literature, the interaction with this positive area in molecules covalently bound is justified by several concepts: charge transfer, dispersion forces, polarization, electrostatic forces, etc. Nevertheless, the meaning of all these models is overlapping, and a great confusion can derived. Indeed, they represent just a dissection of one and unique measurable property, so experimentally measurable, the interaction energy ΔE between two components A and B given by:

$$\Delta E = E(AB) - [E(A) + E(B)] \qquad \text{eq.2}$$

Where E(AB) is the energy of the complex AB, and E(A) and E(B) are the energies of the isolated components. This energy is a consequence of the action of the Coulombic forces that encompass all the forces listed before. Thus, whatever is the cause of the σ-holes interactions, their nature is a consequence of the action of the Coulombic forces

1. 4.4 Donor Molecules in Halogen bond systems

Controlling the arrangement of small molecules in crystalline solids remains a challenge for materials chemistry.[58] More specifically, the importance of establishing a ranking of moieties with similar chemical behaviour has a fundamental role in supramolecular chemistry, where a detailed knowledge of intermolecular interactions, is crucial for the rational preparation of a material with desired structure and properties.[59] Supramolecular interactions such as hydrogen bonding, π stacking represent the most common noncovalent tools in designing novel crystalline architectures. Contrary, halogen bonds have just recently gained the attention as potential guides for the formation of crystals with specific structures. As already observed, a halogen bonding involves an electron-deficient halogen atom and an electron-donating group.[60] Almost any electronegative molecule can act as XB acceptor.[61] For example, the nitrogen atoms of the tetracoordinated

hexamethylenetetramine molecule are good XB acceptor sites.[49,62] Anions are considered to be better halogen-bond acceptors than neutral species.[63] Even cyanometallates have been employed for obtaining strong halogen interactions.[64]

A key role for the formation of this new type of noncovalent interaction is played by the XB donor molecules. Their performance depends on the ability of the halogen atom to be polarized, as well as on the presence of electron-withdrawing moieties that enhance the anisotropy of the electron distribution on the adjacent halogen atom.[59]

According to this information, it is possible to trace a ranking for the XB donor moieties ability following two main guidelines:

a) The power of the XB donor moiety decreases in the order I>Br>Cl>>F.[57]

b) The greater the electron-withdrawing ability of the backbone of the XB donor molecule is, the more effective the XB donor moiety is expected to be.

Aakeröy et al.[59] attempted to rank the interacting preference of chemical moieties by examining six XB donors, carrying different electron withdrawal groups, and their ability to form halogen bonds. The donors molecules are reported in Figure 15 with the correspondent values of the $V_{S,MAX}$ calculated on the surface of the halogen atoms through DFT calculations. Halogens with weak electron withdrawal moieties displayed low electrostatic potential' values. So a first theoretical ranking of XB donor molecules strength was delineated. In order to confirm this hierarchy, the molecules were combined with several XB acceptors to obtain co-crystals. As expected, just the strongest XB donor molecules were able to interact through XBs.

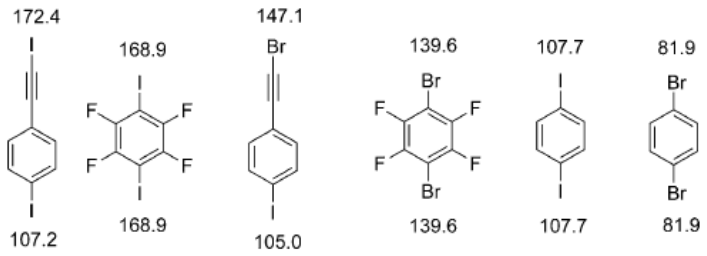

Figure 15 - From left to right: the six XB donor molecules in order of decreasing electrostatic potential, associated with the most positive σ-hole among the halogen atoms in these molecules. Maximum values associated with each XB donor are reported near the corresponding atom. Values are in kJ/mol. Calculation performed through DFT method.[59]

Generally, perfluorohalocarbons (PFHCs) are considered strong halogen bonds donors.[63] Resnati and Metrangolo described the first case of perfluorocarbon – halocarbon (PFC-HC) self-assembly to give co-crystals through interactions between nitrogen as a donor (Lewis base) and iodine as an acceptor (Lewis acid).[65]

One more class of possible XB donors is represented by the N-halosuccinamides. This type of interaction is recognizable in the crystal structure of N-chlorosuccinamide between the chlorine atoms and the carbonyl oxygens.[66] Rissanen and co-workers[49,62] have already employed N-bromosuccinamide and N-iodosuccinamide obtaining robust supramelocular architectures.

This paragraph gives an overview of several XB donor molecules applied for the assembly of novel structures. In this perspective, even if difficult to define, a hierarchy among the several XB donor molecules is fundamental in the supramolecular synthesis of complex architectures.

1. 4.5 Halogen bond versus Hydrogen bond

According to the IUPAC definition, the hydrogen bond is an attractive interaction between a hydrogen atom from a molecule or a molecular fragment R-H in which R is more electronegative than H, and an atom or a group of atoms in the same or a different molecule, in which there is evidence of bond formation.[67] Generally, the formation of a hydrogen bond is indicated by the scheme R-H···Y. As the XB, even in this case the linearity and the distance from the Y atom are indicators of the bond strength. The closer the angle is to 180°, the shorter is the H···Y distance and, so, the stronger is the hydrogen bond.

This type of noncovalent interaction shows lots in common with the XB. In fact, by a computational analysis of the hydrogen atom covalently bound to other more electronegative atoms, it is possible to observe the existence of the σ-hole. Since a hydrogen atom has only one valence electron that is participating in the R-H bond, the outer portion of the hydrogen has a positive potential with its maximum along the extension of the R-H bond (σ-hole).[55] Nonetheless, the lack of any other valence electron on the hydrogen makes its lateral sides to possess a low electron density. Therefore, hydrogen σ-holes are more hemispherical as shown in figures 13 and 16. The hydrogen bonds tend to be not as directional as other σ-hole interactions. This difference

is one of the main from the halogen bonding but not the only one. Indeed, halogenated organic fragments are not readily miscible in aqueous or polar solvents resulting hydrophobic. In particular, it has been demonstrated that polar solvents, such as water, have little influence on the interaction energies and geometries of halogen-bonded adducts in solution.[56] In the case of hydrogen-bonded adducts, the competition with hydrogen bond-donor/acceptor solvents influences their formation. It is possible to define the halogen bonding as the hydrophobic equivalent of the hydrophilic hydrogen bonding.[68] This feature can be exploited in drug design and, so, control the lipophilicity of the drugs for absorption, biological barrier permeability, transport into organs and cells, and interaction with target molecules.[69]

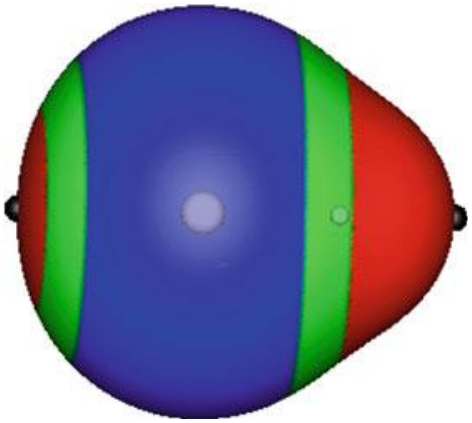

Figure 16 – DFT calculations of the electrostatic potential on the molecular surface of HI. The hydrogen is on the right. The positions of the nuclei are indicated by the light circles. Color ranges, in volts: red, greater than 0.43; green, between 0.43 and 0; blue, less than 0 (negative).[55]

As hydrogen bonds show some differences with the halogen bonds, what happens if they participate together in the assembly of a supramolecular structure? Do they compete or perform a complemental work? These questions are fundamental to predict which will be the primary interaction in a supramolecular system.[70] In the work of Aakeröy *et al*.[70] a wide range of ditopic molecules carrying both a hydrogen and a halogen bond donor (Fig. 17a) were combined with three types of acceptors, monotopic, ditopic symmetric and ditopic asymmetric molecules (Fig. 17b). After co-crystallization, three different plots were obtained. In Figure 18 the diagrams show the preference of interaction in the co-crystallization with the monotopic, ditopic symmetric and ditopic asymmetric acceptor molecules. In the case of monotopic the main supramolecular

interaction is of hydrogen type. Just in a small amount of motifs both XB and HB, contribute for their formation. Passing to the symmetric ditopic until the asymmetric ditopic acceptor molecules, the complemental character of each interaction increases. The crystals are formed with the co-participation of both bonds. Nevertheless, the study has shown that hydrogen bonding is likely to be more effective as synthetic vector.

(a)

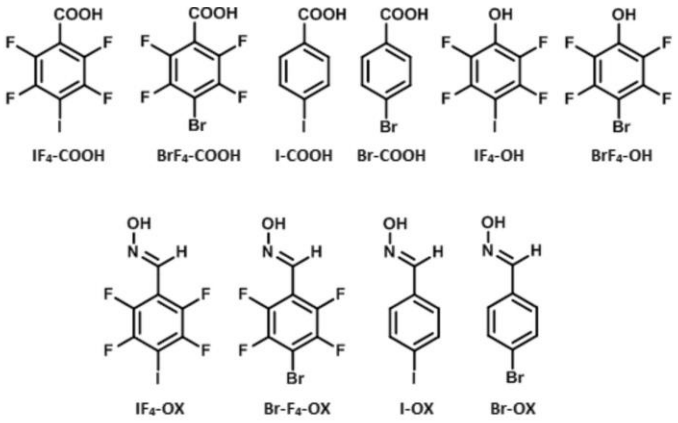

b)

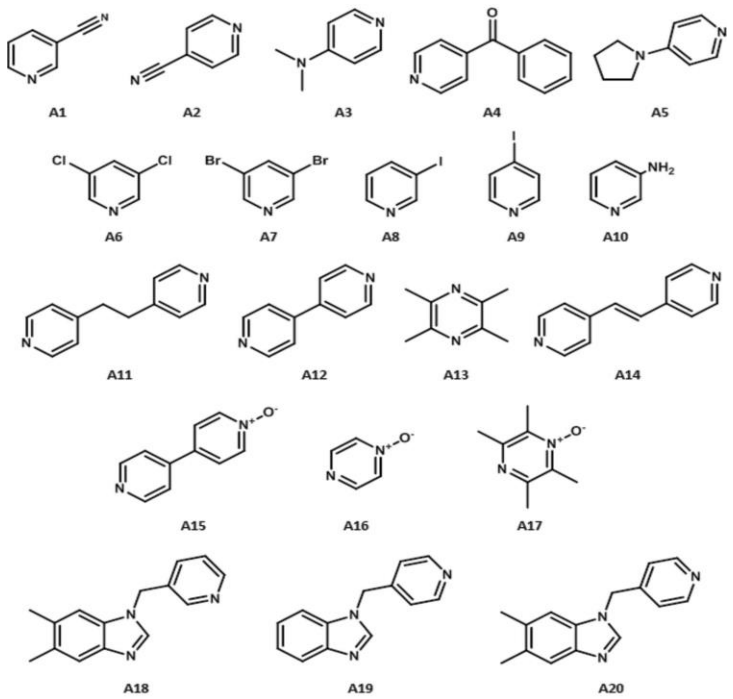

Figure 17 - (a) Bifunctional hydrogen and halogen bond donors, and (b) acceptor molecules.[70]

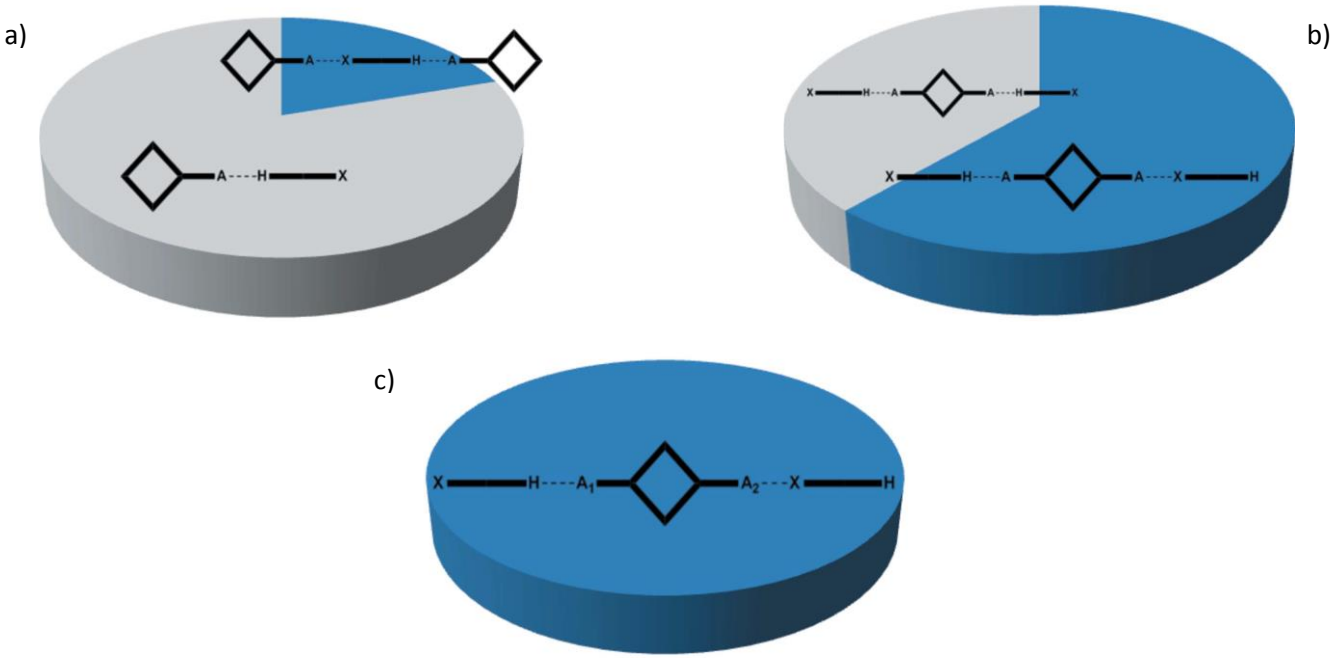

Figure 18 - Diagrams that represent the preference of interaction in the co-crystallization with the monotopic (a), ditopic symmetric (b) and ditopic asymmetric (c) acceptor molecules.[70]

In another study carried on by Raatikainen *et al.*[71] several simple haloanilinium and halopyridinium salt structures (Fig. 19) were described showing the balance between HB and XB in the solid state. For all the haloanilinium compounds, the hydrogen bonding is the major responsible for the crystal packing. If in structures 1 to 3 and in structure 5 XBs slightly contribute for the motif complexation in structure 4 do not participate. The same plot appears for structures where the chlorine anion is substituted with dihydrogen phosphate groups. Indeed, hydrogen bond dominates the crystal packing. Differently, passing from haloanilinium to halopyridinium salts the XB competes with the HB, and in the case of structure 9 the entire architecture is built up through XBs.

The different studies confirm that halogen bonding is acquiring more and more importance in tailoring the properties of new supramolecular architectures.

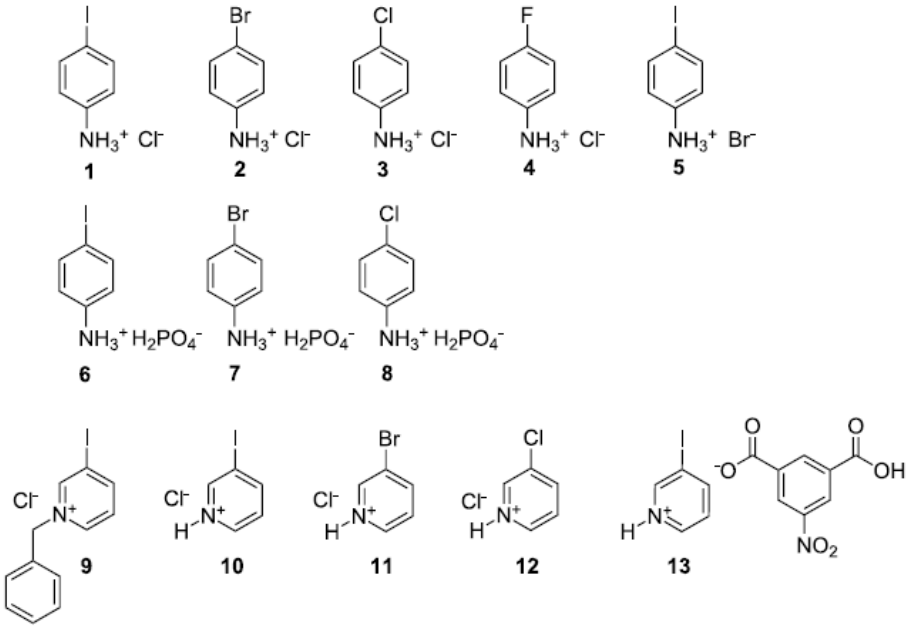

Figure 19 - Chemical structures of the salts: from 1 to 8 haloanilinium salts; from 9 to 13 halopyridinium salts.[71]

1. 5.1 Single crystal X-Ray Diffraction

Before presenting the developed project, a paragraph is dedicated to the importance of single crystal phase study, as the entire work came out from the analysis of several single crystals obtained from solution.

First, it is mandatory to specify what a crystal is:

''A crystal is an anisotropic, homogeneous body consisting of a three-dimensional periodic ordering of atoms, ions or molecules''[72]

A typical material is composed of many smaller crystals of which boundaries influence its properties. From a research point of view, especially when creating a new material, scientists want to remove as many variables as possible to understand the properties of the materials. To obtain this, materials have to be studied as pure as possible, and here it comes clear the importance of single crystals where impurities and defects have been radically reduced.

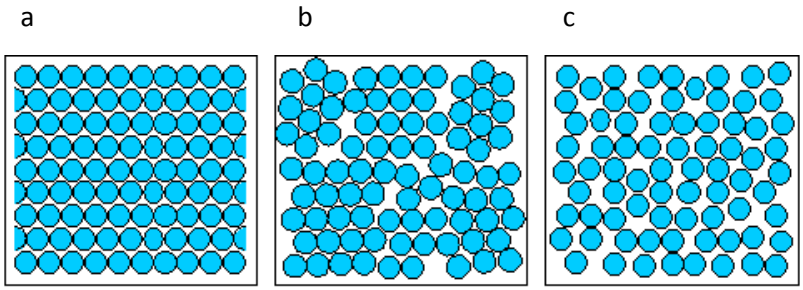

Figure 20 - Representation of the three phases in the solid state: single crystal (a), polycrystalline material (b) and amorphous phase (c).[73]

Figure 20 shows the difference between single crystals, polycrystalline materials, and amorphous phases. In single crystals, a long-range order of atoms exists. In the case of polycrystalline materials, defined regions with their own order of atoms coexist. Regarding amorphous materials, no order can be found.

Thus, single crystals play a decisive role not only in the context of complex materials research. Single-crystal X-ray structural analysis still represents the definitive proof of a structure for the chemists. The discussion of molecular and other properties depends upon it, especially for a comparison with structures calculated from quantum chemistry.[74]

1. 5.2 Crystal Parameters

As a crystal is a solid where a pattern is repeated over the three dimensions, it is necessary just to know its motif to describe the entire structure. The motif can be converted by symmetry operations along three spatial vectors a, b, c, forming, thus, a lattice. The smallest unit volume of that is called the unit cell. It is described by the three lattice constants a, b and c (length of the basis vectors) and the angles formed by them α, β and γ (Fig. 21).

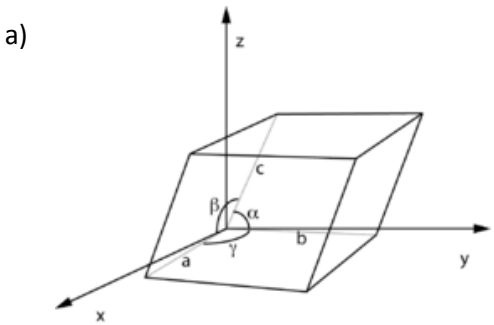

b)

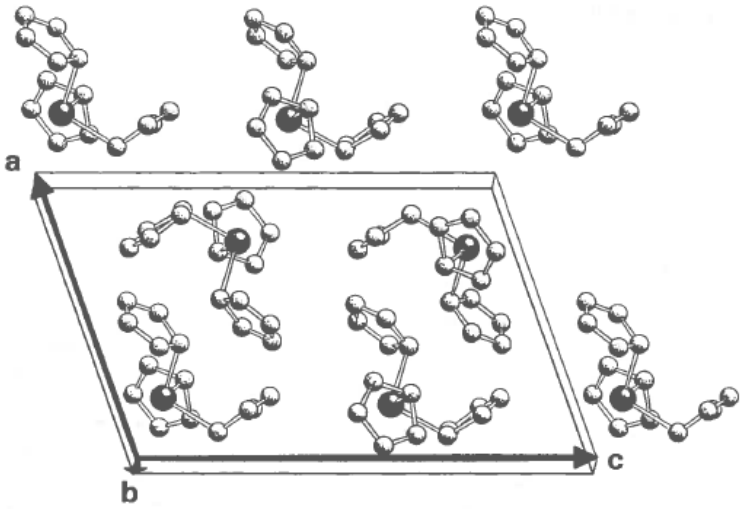

Figure 21 – Unit cell parameters (a) and an example of the unit cell in crystal packing (b).[75]

A crystal possesses one more property than periodicity, symmetry. Full consideration of all possible symmetries in a lattice gave rise to seven possibilities, the seven crystal systems (Table 2).[75]

Table 2 - The seven crystal systems.[75]

Cell system	***cell edges***	***cell angles***	***essential symmetry***
Triclinic	a ≠ b ≠ c	α ≠ β ≠ γ	none
Monoclinic	a ≠ b ≠ c	α = γ = 90°	1xC_2-axis
Orthorhombic	a ≠ b ≠ c	α = β = γ = 90°	3x perpendicular C_2-axis
Tetragonal	a=b	α = β = 90°	1xC_4-axis
Trigonal / Hexagonal	a=b=c	α = β = 90°, γ = 120°	1xC_3/1xC_6-axis
Cubic	a=b=c	α = β = γ = 90°	4xC_3-axis

The unit cell has to be chosen in such a way that the highest number of symmetries is described. Sometimes just the seven crystal systems are enough for that description. They are also called primitive cells, indicated by the P letter, to be distinguished from the centred ones. The latter are used when better describe the symmetry of a crystal even if this implies the consideration of more lattice points. Centred cells are indicated by letters I (body-centred), A, B, C (based-centred), and F (face-centred). Thus, the lattice systems used to describe crystals are 14, recognized as the 14 Bravais Lattices (Fig. 22).[72]

In the atomic lattice of a crystal it is possible to recognize the existence of parallel planes formed by the lattice points. The orientation of such planes is defined by the Miller indices with the values h, k, and l. These can be determined by recognizing the plane that lies nearest to the origin of the unit cell. Thus, the reciprocal of the intercepts between the plane and the axis of the unit cell, a, b and c, correspond to the h, k and l values and they are always integers.

Once presented the parameters of the base structure of a crystal, the section continues showing some important topics of crystallography. These are presented roughly, as the main object of the entire project was the development of novel nanoporous materials.

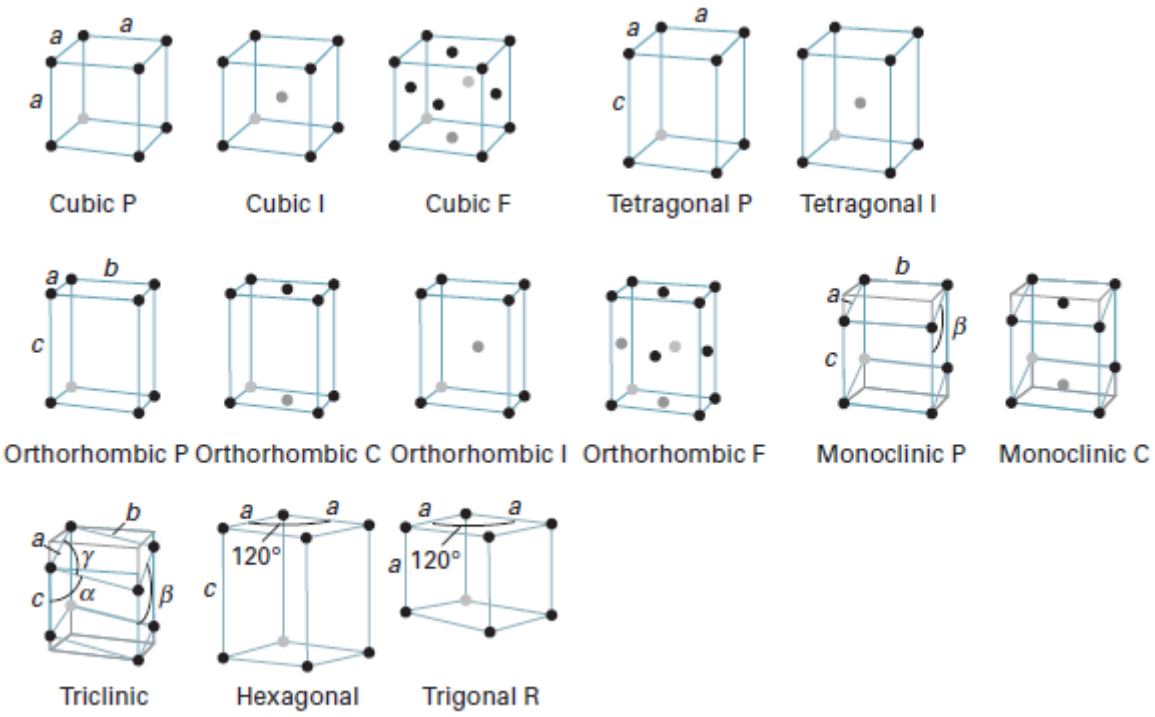

Figure 22 - Representation of the 14 Bravais lattices.[76]

1. 5.3 X-Ray diffraction

Crystallography finds its origin on the discovery of X-rays by Wilhelm Conrad Röntgen who received the Nobel Prize in physics at 1901.

X radiations are emitted when the electrons change the energy state. Generally, X-rays have a wavelength ranging from 0.01 to 10 nm of the electromagnetic spectrum, resulting highly energetic and penetrating radiations. For this reason, they are good for interacting at the atomic level, penetrating the lattice planes of a crystal.

After their discovery, different scientists contributed for the evolution of crystallography. Max von Laue managed to produce a diffraction pattern investigating the interaction between X-Rays and crystals. He found that crystals are composed by periodic arrays of atoms (Fig. 23), and cause X-Rays diffraction patterns due to the atoms and their 3-dimensional spacing.

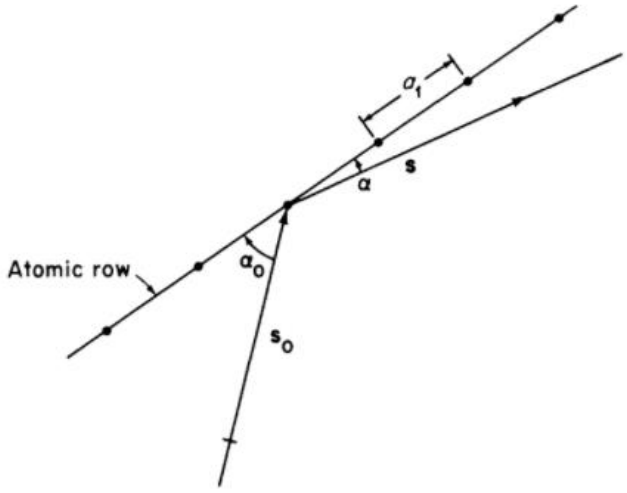

Figure 23 – Laue model of the diffraction by a row of atoms.[77]

One of the major contributions came with Bragg family, father and son, who, based on the work of Laue, formulated the relationship between crystal's atomic structure and its X-Ray diffraction providing a tool which has revolutionized our understanding of matter.[72]

$$n\lambda = 2d_{hkl}(\sin\theta) \quad (n=1, 2, 3,\ldots) \qquad \textit{Bragg's Law} \qquad \text{eq. 3}$$

Where λ is the wavelength, d_{hkl} is the spacing between atomic planes and θ is the angle between the incident rays and the surface of the crystals. Figure 24 shows the mechanism that brought to the formulation of this law. When a beam of X-rays irradiated a substance, the X-ray reflected from the surface of that substance has less traveled than one that is reflected from the atomic planes in the bulk. This means that the two waves have a difference in their reflection path. This difference is related to the planes distance, d_{hkl}, and the angle at which the X-ray penetrates into the material. The two waves are in phase if the one reflected from the atomic layers has traveled a whole number of wavelengths while inside the material. Thus when n is an integer, the reflected waves from different atomic planes are in phase, and a constructive interference is produced. In case n is not an integer, destructive interference occurs, and no diffraction pattern is produced.

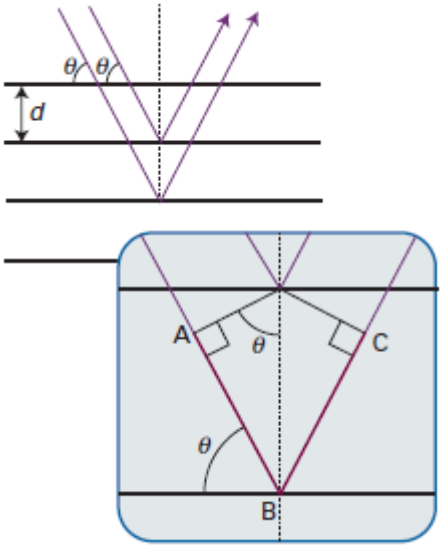

Figure 24 - Bragg's Law representation: the path length difference between X-rays hitting parallel atomic planes has to be a multiple of their wavelength.[76]

In order to analyse crystals, X-ray diffractometers are fundamental. They consist of three basic elements, an X-ray tube, a sample holder, and an X-ray detector.[75] In the cathode tube, X-rays are produced by the impact of electrons on a target. The electrons are formed after heating a filament and applying a voltage that accelerates them to the target. Electrons with enough energy can rip electrons of inner shells of the target, and, so, X-rays spectra are produced (Fig.25).

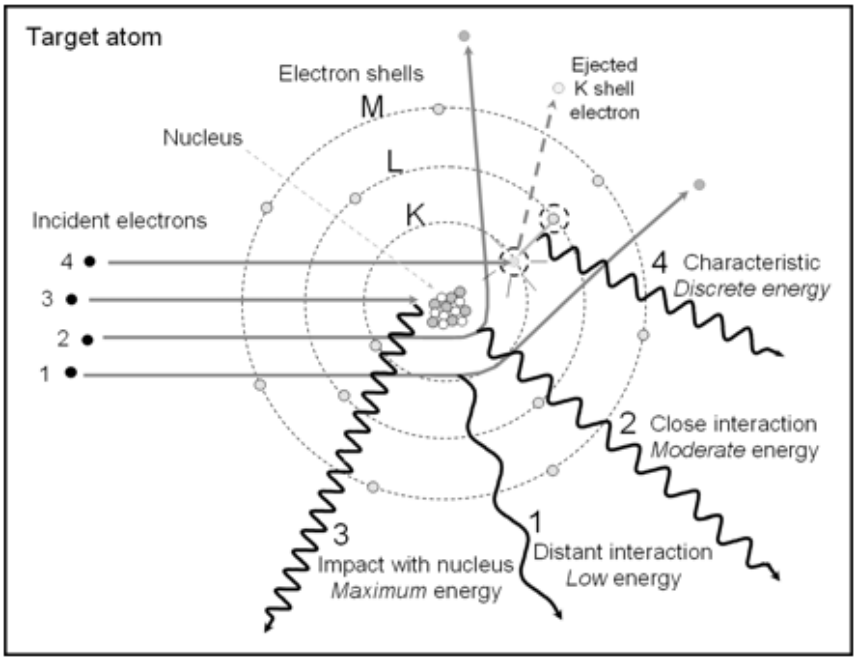

Figure 25 - X-ray production through quantum phenomena explanation.[78]

Many electronic transitions occur in the atoms when the target is stricken so that many wavelengths are produced from the atomic shells. Consequently, in the spectra, several components will be present. As the Kα radiations (from the Kα shell) are the most energetic, in order to obtain the right diffraction intensities, some filters are applied such as foils or crystals monochrometers that absorb the wavelengths less energetic than Kα. The most common targets used for the production of X-rays are Molybdenum and Copper. The Kα radiations produced by Molybdenum and Copper have wavelengths of 0.7107Å and 0.15406 Å respectively. Once produced, X-rays are directed to the sample. When the geometry of the incident X-rays against the sample satisfies the Bragg Equation, constructive interference occurs. The detector collects the signal of the diffracted X-rays, converts it into a count rate and sends it to a device such as a computer monitor.

Both powder X-ray diffractometers and single crystal X-ray diffractometers have similar instrumentation. Nevertheless, in the single crystal case, the diffractometers use either 3- or 4-circle goniometers. These circles refer to the four angles (θ, χ, φ, and Ω) that define the relationship between the crystal lattice, the incident ray and the detector.[75] Samples are mounted

on thin glass fibers that are attached to brass pins and mounted onto goniometer heads. Adjustment of the x, y and z orthogonal directions allows the centering of the crystal within the X-ray beam (Fig. 26).

When radiation hits the single crystal, three following phenomena occur: transmission, reflection, and diffraction. A beam stopper blocks the transmitted radiations to avoid the burning of the detector. The detector due to the angles involved does not pick up the reflected rays. Just the diffracted rays are collected.

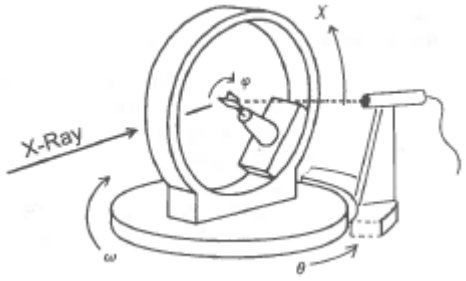

Figure 26 - Schematic representation of single crystal X-ray diffractometer.[75]

1. 5.4 Single crystal growth

The goal in growing crystals for a single crystal X-ray diffraction experiment is to grow single crystals of suitable size. The optimum size for a crystal is one that has dimensions of 0.2 - 0.4 mm in at least two of the three dimensions.

Crystals and single crystals are obtained depending on the relative rate of nucleation and growth. A fast nucleation means really small crystals or agglomerates. On the other hand, fast rate of growth implies the inclusion of defects in the crystal structure. The right compromise for a perfect single crystal has not been discovered. Anyway, different crystallization methods have been developed.

Most of the single crystals are obtained from solution. When a solution is oversaturated the crystal precipitates out. There are numerous factors during crystal growth, which affect both the size and the quality of the crystal. The most important are purity of compounds, crystallization

solvent, number of nucleation sites, mechanical agitation applied to the system, and time.[79] Several techniques of crystal growth from solution exist. Herein, just some of them are presented.

Slow evaporation (Fig. 27a) is the simplest one and consists of the preparation of a suitable solution with the desired compounds. This is left in a clean container, with a large surface and not tightly covered to favour solvent evaporation. To avoid a fast nucleation, the sample is subjected to the less disturb as possible. The performance of this technique is easy but the probability to obtain small crystallites or agglomerates is high as the oversaturation point is rapidly reached.

Vapour diffusion (Fig. 27b) is a method that needs a binary system of solvents. Both solvents have to be miscible one to each other, but with different boiling points. The one with the higher boiling point is called solvent, and that with a lower boiling point is called precipitant. The compound has to be dissolved in the solvent. After transferring the mixture in a vial, this is put in a container with the precipitant, and sealed. Over the time, the precipitant, which is more volatile, will diffuse over the gas phase into the solvent, leading to oversaturation, nucleation and, if all goes well, finally crystallization.[79]

Liquid-liquid diffusion (Fig. 27c) even in this technique a binary solvent system is necessary. Differently, from the previous method, the two solvents have different densities. Once the solution with the proper compound is ready, the second solvent with a different density is gently poured over that with a syringe to avoid the immediate mixture of the two liquids. Over the time, the solvents will mix and crystals will be formed.

Finally, in *slow cooling* method (Fig. 27d*)* a nearly saturated solution of the compound or close to the boiling point of the solvent is prepared. Afterwards, it is transferred to a clean container and covered. This is placed in a heat bath at about the same temperature and left to cool down slowly.
The above-listed methods single crystals growth are all from solution. It is possible to obtain single crystals both from melt solutions and from gas phases[75] but for the present project, they were not taken into consideration and, thus, they are not explained.

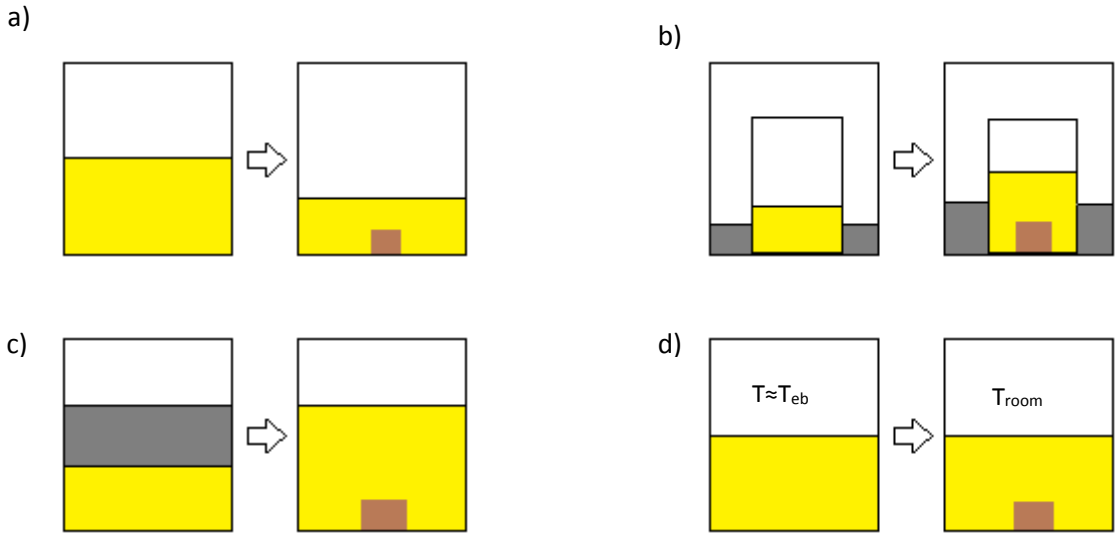

Figure 27 - Representation of the several single crystal growth methods from solution; slow evaporation (a); vapour diffusion (b); liquid-liquid diffusion (c); slow cooling (d).

1. 6 Objectives of the work

The main object of this study was to achieve the complexation of a tetracoordinated motif through the tetrafunctional Lewis base hexamethylenetetramine (HMTA) to give nanoporous structures. This tetradentate base has been exploited in previous works combined with Ag(I) salts in order to produce supertetrahedral networks with large interstitial cavities.[80]

On this purpose, the first goal was to examine the affection of XBs on the crystal packing by changing the XB donor molecules. Based on the past works of Raatikainen *et al,*[49,62] the first molecules used as XB donors were NCS, NBS, and NIS. We probed the nucleophilicity of nitrogen atoms on HMTA molecule even with molecular iodine and iodopentafluorobenzene molecule. One more object was to verify the existence of easier ways to obtain the tetracoordinated complex. According to the mechanochemistry' rules,[81] we combined N-halosuccinamide with one more molecule acting as less active XB donor or as stronger XB donor.

The strength of the interactions between the halogen and the electronegative atoms of the XB acceptor were measured by considering their distance normalized according to the van der Waals radii through the formula:

$$R = d / (r_x + r_N) \qquad \text{eq. 4}$$

where r_x and r_N are the vdW radii of the halogen and the nitrogen respectively (Table 7, Annexes).[82]

All structures were obtained by crystallization methods from solution. Even if the real influence of the solvents on the halogen bonds is not still stated, it has been deduced[83] that complexation through halogen bonds recognition occurs in apolar and aprotic polar solvents. According to this consideration, we used apolar and aprotic polar solvents to verify the minimum competition between halogen and hydrogen interactions.

2. Experimental section

2.1 Reagents and solvents

Reagents and solvents used in the experimental part are listed in Table 3.

Table 3 - Reagents and solvents used in the experimental part.

Name	***Supplier***	***Purity grade***
Acetone	VWR®	99.9%
Acetonitrile	Fisher®	99.9%
Chloroform	Fisher®	99.9%
1,3-Dibromohydantoin	Sigma Aldrich®	98%
Dichloromethane	VWR®	≥ 99.9%
Hexamethylenetetramine	Sigma Aldrich®	99.5%
Iodine	TCI®	98%
Iodopentafluorobenzene	TCI®	95%
N-bromophthalimide	Sigma Aldrich®	95%
N-bromosuccinimide	Sigma Aldrich®	99%
N-chlorosuccinimide	Sigma Aldrich®	98%
N-iodosuccinimide	TCI®	98%
Nitromethane	J.T. BAKER®	95%
1,2-Nitropropane	J.T. BAKER®	96%
Tetrachloromethane	VWR®	≥99.5%
Toluene	VWR®	≥ 99.9%

All the solvents used for synthesis and crystal growth were reagent grade and were used as received.

2. 2 Synthesis of $(HMTA^{-}CH_2OH)^{+}Cl^{-}$

To HMTA (10 mg, 0.071 mmol) dissolved in ACN (1.0ml) and chloroform (1.0 ml), a solution of NCS (75.85 mg, 0.568 mmol) in chloroform (2.0 ml) was added dropwise at room temperature. The final colourless solution protected from light was subjected to slow evaporation at room temperature to give colourless crystals (Scheme 1).

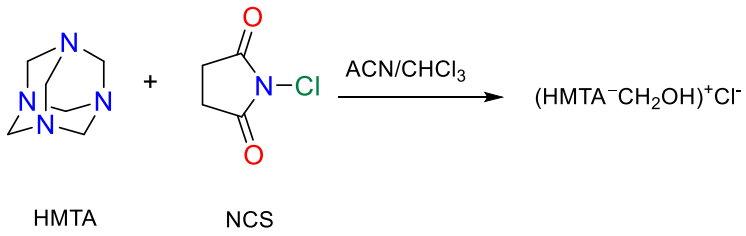

Scheme 1: ChemDraw representation of chemical reaction between NCS and HMTA.

2. 3 Synthesis of $(HMTA)Br_2$

Method 1: To HMTA (20.0 mg, 0.143 mmol) in ACN (10.0 ml), was added a colourless solution of NBS (101.80 mg, 0.572 mmol) dissolved in ACN (10.0 ml) (Scheme 2a). After the formation of white precipitates, the solution was filtered. The resulting yellow coloured solution was subjected to hexane vapor diffusion to give colourless crystals.

Method 2: Solid NBS (101.80 mg, 0.572 mmol) was added to HMTA (20.0 mg, 0.143 mmol) dissolved in chloroform (20.0 ml). In three different experiences, one or two more solvents were separately layered over the previous solution at room temperature (Table 4). The resultant solutions were subjected to hexane vapor diffusion to give colourless crystals.

Method 3: Solid 1,3-Dibromohydantoin (81.20 mg, 0.284 mmol) was added to HMTA (10.0 mg, 0.071 mmol) dissolved in ACN. After the formation of white precipitates, the solution was filtered.

The resulting clear filtrate solutions were subjected to hexane vapor diffusion (Scheme 2b) to give colourless crystals.

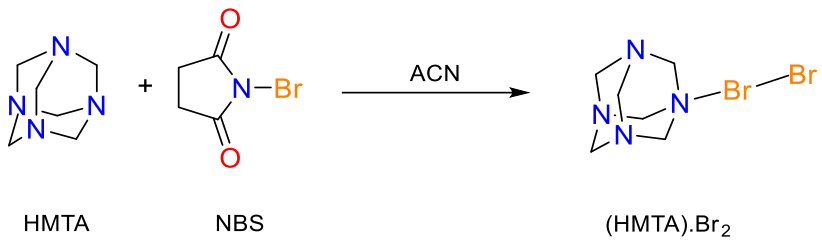

Scheme 2a: ChemDraw representation of chemical reaction between NBS with HMTA.

Table 4 - List of solvents combination with the relative ratios for the synthesis of $(HMTA)Br_{2.}$

HMTA+NBS/ Solvent 1	Solvent 2	Solvent 3	Volumes' ratios
$CHCl_3$	2-Nitropropane	/	1:1
$CHCl_3$	CCl_4	2-Nitropropane	1:1:1
$CHCl_3$	CCl_4	Nitromethane	1:1:1

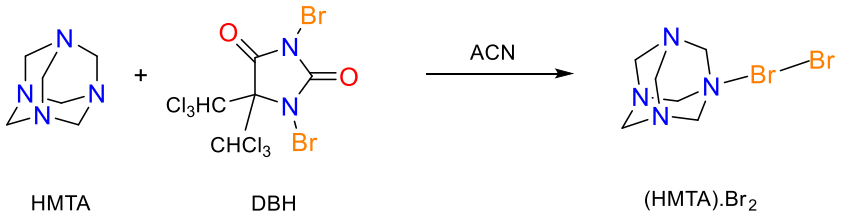

Scheme 2b: ChemDraw representation of chemical reaction between DBH with HMTA.

2. 4 Synthesis of (HMTA)•2(C_6F_5I)

To HMTA (5.0 mg, 0.036 mmol) dissolved in ACN (1.0 ml) was added C_6F_5I (84.66 mg, 0.288 mmol) at room temperature. The colorless solution was subjected to slow evaporation (Scheme 3) to give colourless crystals.

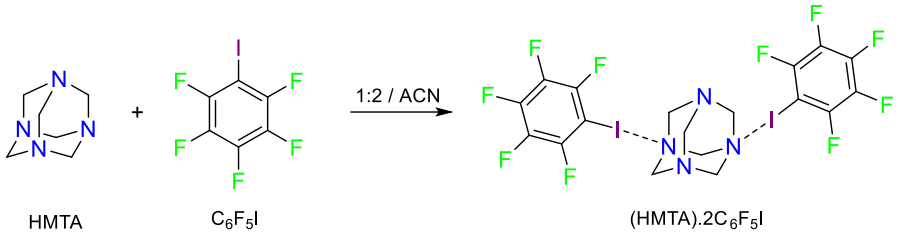

Scheme 3: ChemDraw representation of chemical reaction between iodopentafluorobenzene and HMTA.

2. 5 Synthesis of (HMTA)•2(I_2)

To HMTA (10 mg, 0.071 mmol) dissolved in chloroform (4.0 ml), iodine (71.51 mg, 0.284 mmol) dissolved in chloroform (7 ml) was added at room temperature. The final purple red coloured solution was left at room temperature protected from light, and subjected to slow evaporation (Scheme 4).

Alternate method: To 5 mg of HMTA (0.036 mmol) and 72.52 mg of iodine (0.288 mmol) taken in a mortar, three drops of either dichloromethane or chloroform were added. The mixture was ground finely. The purple-red powder was transferred into a 20.0 ml vial and dissolved in 15 ml of either dichloromethane or chloroform. The solutions were subjected to hexane vapour diffusion.

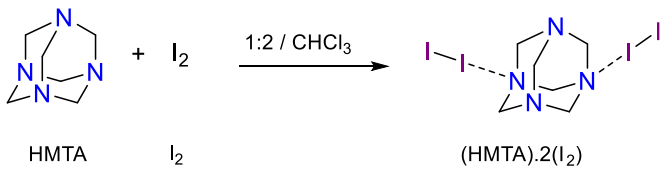

Scheme 4: ChemDraw representation of chemical reaction between Iodine and HMTA.

2. 6 Synthesis of (HMTA)•2(BrCl)

To NBS (50.54 mg, 0.284 mmol) dissolved in ACN (1 ml), NCS (37.92 mg, 0.284 mmol) dissolved in 1.0 ml of ACN was added at room temperature. The resultant solution was added

dropwise to HMTA (10 mg, 0.071 mmol) dissolved in ACN (2.5 ml) at room temperature (Scheme 5). The final colourless solution was left for slow evaporation to give colourless crystals.

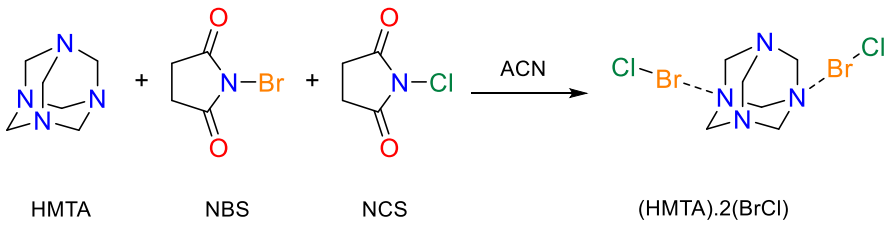

Scheme 5: ChemDraw representation of chemical reaction between NBS with NCS and HMTA.

2. 7 Synthesis of (HMTA)•2(ICl)

Method 1: 2.0 ml of a mixture of NIS (63.89 mg, 0.284 mmol) dissolved in ACN (1ml) and NCS (37.92 mg, 0.284 mmol) dissolved in ACN (1ml) were prepared. The NIS-NCS mixture was added dropwise to HMTA (10 mg, 0.071 mmol) dissolved in ACN (2.5 ml). After few drops, precipitation occurred. The solution was filtered and left to evaporate slowly at room temperature (Scheme 6) to give colourless crystals.

Method 2: 5 mg of HMTA (0.036 mmol), 70.51 mg of iodine (0.288 mmol) and 34.46 mg of NCS (0.288 mmol) with three drops of nitromethane were taken in a mortar and were finely ground. The green powder was transferred to a 20.0ml vial, and dissolved using 15 ml of nitromethane, and subjected to hexane vapor diffusion to give colourless crystals. The procedure using ACN instead of nitromethane yielded a similar complex.

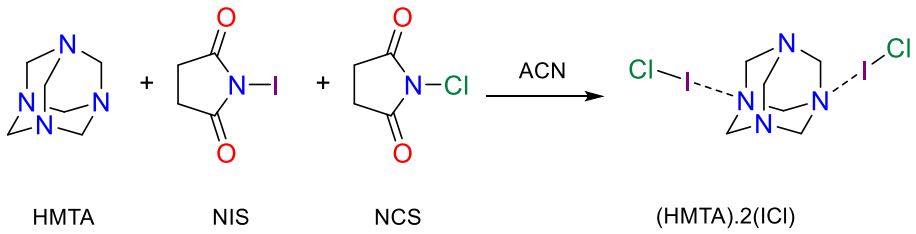

Scheme 6: ChemDraw representation of chemical reaction between NIS with NCS and HMTA.

2. 8 Synthesis of (HMTA)•2(NBP)

White powder precipitates and small crystals started to form immediately by adding NBP (32.54 mg, 0.144 mmol) dissolved in ACN (5.0 ml) dropwise to HMTA (5.0 mg, 0.036 mmol) dissolved in warm ACN (5.0 ml). The solution was allowed to slowly evaporate at room temperature (Scheme 7) to give colourless crystals.

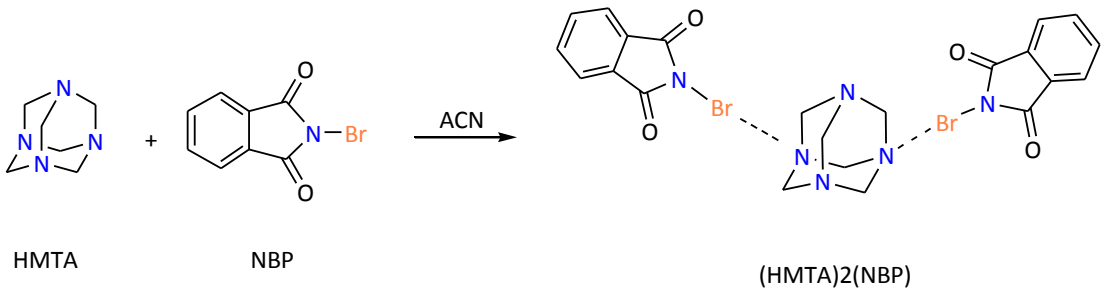

Scheme 7: ChemDraw representation of chemical reaction between NBP and HMTA.

2. 9 Synthesis of solvated (HMTA)•2(NBS)

To HMTA (20 mg, 0.143 mmol) dissolved in chloroform (22 ml), solid NBS (101.80 mg, 0.572 mmol) were added in portions. Solid NBS dissolution required exhaustive shaking. The clear yellow solution was subjected to hexane vapor diffusion. In further experiences, similar results were obtained by layering separately one or two more solvents over the clear yellow solution (Table 5) and leaving the resulting solutions for vapor diffusion with hexane (Scheme 8).

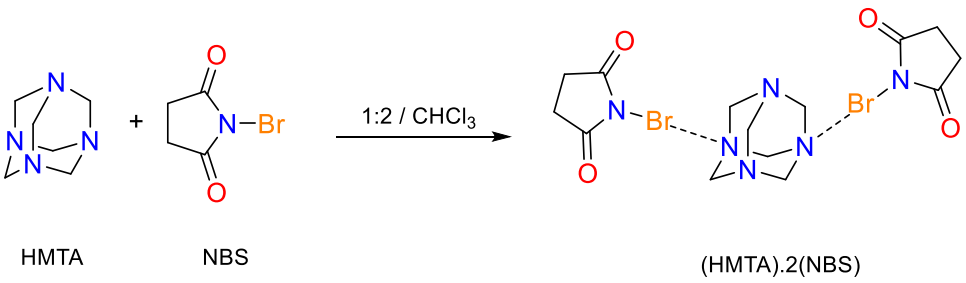

Scheme 8: ChemDraw representation of chemical reaction between NBS and HMTA.

Alternate method: 5mg of HMTA (0.036 mmol), 25.63 mg of NBS (0.144 mmol) and three drops of dichloromethane placed in a mortar were finely ground. The yellow powder was transferred in a 20.0ml vial and dissolved in chloroform (7 ml) and subjected to hexane vapor diffusion.

Table 5 - List of solvents order with the relative ratios for the synthesis of (HMTA)•2(NBS).

HMTA+NBS/ Solvent-1	**Solvent-2**	**Solvent-3**	**Volumes' ratios**
$CHCl_3$	DCM	/	1:1
$CHCl_3$	CCl_4	DCM	1:1:1
$CHCl_3$	CCl_4	DCM	1:0.1:0.9
$CHCl_3$	CCl_4	DCM	1:0.2:0.8
$CHCl_3$	CCl_4	Toluene	1:1:1
$CHCl_3$	CCl_4	Toluene	1:0.1:0.9
$CHCl_3$	CCl_4	Toluene	1:0.2:0.8
$CHCl_3$	CCl_4	ACN	1:1
$CHCl_3$	CCl_4	Acetone	1:1

2. 10 Synthesis of (HMTA)•4(NBS) @CH_2Cl_2

5 mg of HMTA (0.036 mmol), 25.63 mg of NBS (0.144 mmol) and three drops of either tetrachloromethane or toluene or ACN were placed in a mortar and were finely ground. The final yellow powder was dissolved in 5 ml of DCM by exhaustive shaking. The colourless solution left at room temperature was subjected to hexane vapour diffusion to give colourless crystals (Scheme 9).

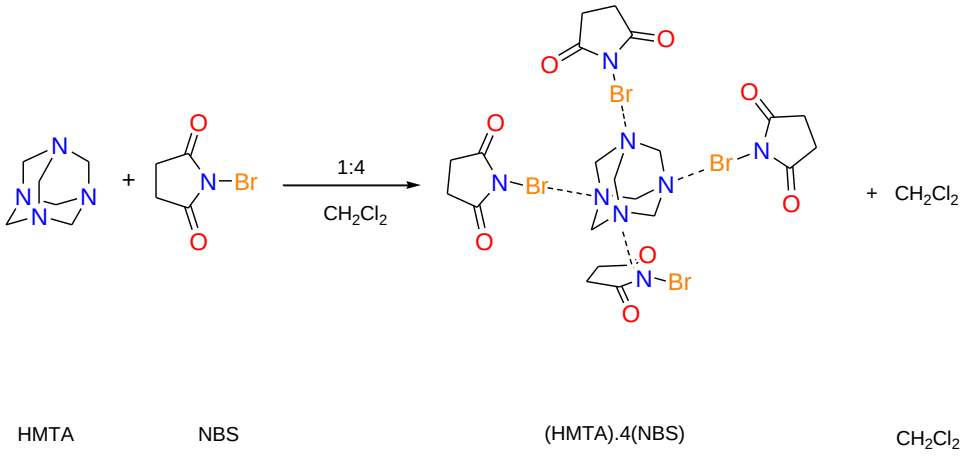

Scheme 9: ChemDraw representation of chemical reaction between NBS and HMTA.

2. 11 Synthesis of (HMTA)•4(NBS)@CCl_4

To HMTA (20 mg, 0.143 mmol) dissolved in chloroform (20 ml), solid NBS (101.80 mg, 0,572 mmol) were added in portions and, solids were dissolved by using exhaustive hand shaking. Then, 20ml of CCl_4 was gently layered using a Pasteur pipette. White solids that formed at the interface between the two solvents gradually disappeared giving a homogeneous solution. The solution subjected to hexane vapor diffusion gave colourless crystalline needles suitable for X-ray analysis (Scheme 10).

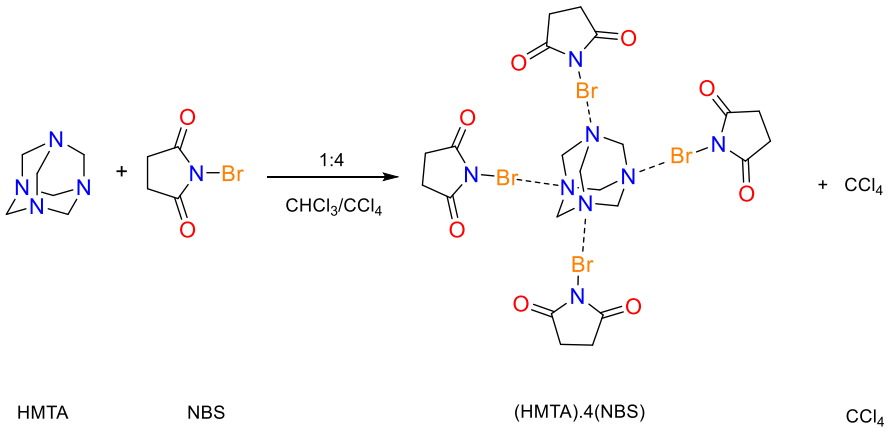

Scheme 10: ChemDraw representation of chemical reaction between NBS and HMTA.

2. 12 Synthesis of (HMTA)•2(NIS)

ACN (13.0 ml) was carefully layered over HMTA (5.0 mg, 0.036 mmol) dissolved in chloroform (13 ml,). A third solution, i.e., NIS (32.40 mg, 0.144 mmol) dissolved in dichloromethane (13 ml) was layered over the previous solution. The resulting solution characterized by two distinguishable layers was subjected to hexane vapor diffusion to give colourless crystals (Scheme 11).

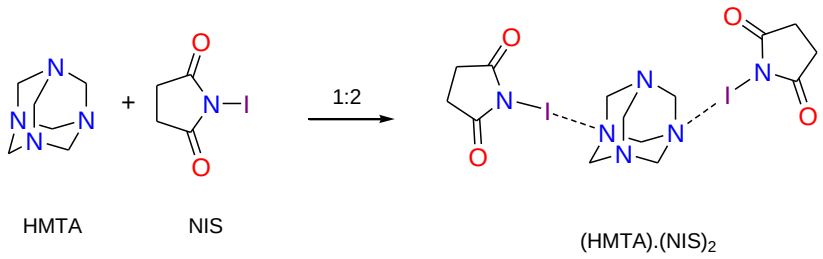

Scheme 11: ChemDraw representation of chemical reaction between NIS and HMTA.

Alternate method: the same procedure was followed by layering different solvents. Table 6 reports the experimental conditions of different trials. In the first case, HMTA was dissolved in chloroform and NIS in Acetone. For all the other cases, both HMTA and NIS were dissolved in ACN.

Table 6 - List of solvents combination with the relative volumes' ratios for the synthesis of (HMTA)•2 (NIS).

HMTA/Solvent-1	Solvent-2	NIS/Solvent-3	Volumes' ratios
$CHCl_3$	ACN	Acetone	1:1:1
ACN	DCM	ACN	1:1:1
ACN	Toluene	ACN	1:1:1
ACN	$CHCl_3$	ACN	1:1:1
ACN	CCl_4	ACN	1:1:1

2. 13 Synthesis of (HMTA)•4(NIS)@CH_2Cl_2

5mg of HMTA (0.036 mmol), 72.52 mg of iodine (0.288 mmol), 38.46 mg of NCS (0.288 mmol) and three drops of the dichloromethane were placed in a mortar and were finely ground. The final green powder was transferred to a vial, and 20 ml of DCM were added. The solids dissolution occurred with exhaustive shaken. The purple red coloured solution was subjected to hexane vapour diffusion (Scheme 12).

The same procedure was repeated using chloroform instead of DCM.

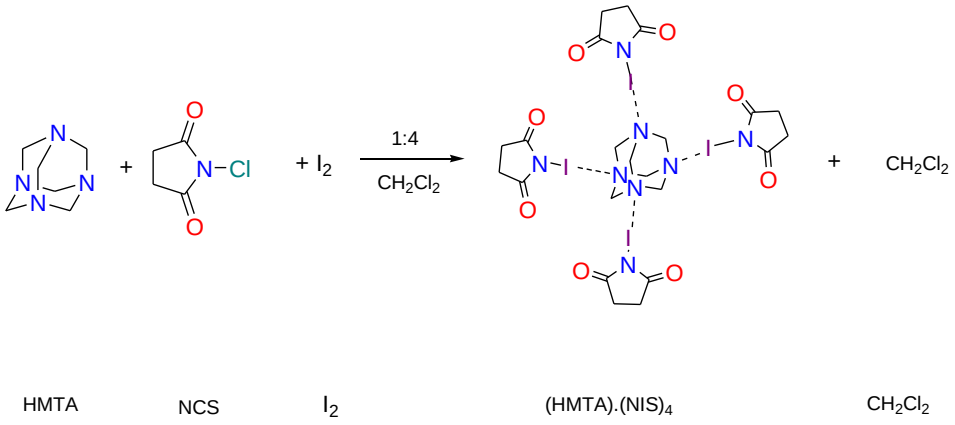

Scheme 12: ChemDraw representation of chemical reaction between Iodine, NCS and HMTA.

2. 14 Crystallographic data

Single crystal X-ray data for **(HMTA-$CH_2OH)^+Cl^-$**, **(HMTA) •2(NBS)**, **(HMTA) • 2(I2)**, **(HMTA) •2(BrCl)**, **(HMTA) •2(ICl),** , **(HMTA) •4(NBS)@CH_2Cl_2**, **(HMTA) •4(NBS)@CCl_4** and **(HMTA) •4(NIS)@CH_2Cl_2**, were measured on a Bruker-Nonius Kappa CCD diffractometer equipped with an APEX-II CCD detector which utilizes graphite-monochromated Mo-Kα (λ = 0.71073 Å) radiation. The data for **(HMTA) •(Br2)**, **(HMTA) •2(C_6F_5I)**, **(HMTA)•2(NBP)** and **(HMTA)•2(NIS)** were measured on a single source Rigaku Oxford diffractometer equipped with an Eos CCD detector using mirror-monochromated Mo-*K*α (λ = 0.71073 Å) radiation. The crystal data and experimental details for the data collections are given in Tables 8-19. Data collection and reduction for Rigaku

Oxford diffractometers were performed using the program *CrysAlisPro*[84] and Gaussian face indexing-based absorption correction method was applied through *CrysAlisPro.*[84] The data collections of Bruker-Nonius Kappa CCD diffractometer were performed using the program *COLLECT*[85] and *HKL DENZO AND SCALEPACK,*[86] and multi-scan absorption correction was applied using *SADABS.*[87] The structures were solved by direct methods with SHELXS,[88] and refined by full-matrix least squares on *F*[85] using the *OLEX2*[89] which utilize the *SHELXL*-2016[88] module. No attempt was made to locate the hydrogens from difference electron density Fourier maps, and appropriate constraints and restraints were used when necessary for disordered molecules.

3. Results and discussion

3.1 Structure $(HMTACH_2OH)^+Cl^-$

The addition of a solution of NCS in chloroform to a solution of HMTA in ACN led to the formation of a salt, Scheme 1.

NCS is used for chlorinations and as a mild oxidant. In fact, it is known to be a good chlorine provider in radical reactions. On the other hand, the high electronegativity that characterizes the chlorine atom makes NCS belonging to the category of weak XB donors. Indeed, it is stated that halogens and derivatives work as XB donors, and the tendency to form strong interactions is I > Br > Cl >> F.[90] For equal electron withdrawal moieties, compared to NBS and NIS, it is less polarizable, and its σ-hole potential is less electropositive. Thus, it is less prominent on interacting as XB donor.

The chlorine anion that forms the salt with the HMTA molecule is provided both from the N-halosuccinamide and from the chloroform. The low polarity of chlorine does not favour XB formation, and as expected, none of the XB interactions is present in the final crystal structure.

3.2 Structure (HMTA) •Br_2

Initially, the HMTA molecule was mixed with NIS in one to four ratios from ACN solution. White powder precipitates were obtained. The fast reaction between the halogen atoms and the nucleophilic sites of HMTA prevented the arrangement of the synthons through hydrogen interactions. The saturated solution precipitated, and white solids appeared.

The substitution of the aprotic polar solvent ACN with others such as acetone, nitromethane, DCM, chloroform, tetrachloromethane, and toluene, either gave white precipitates or decomposed products.

Passing from NIS to NBS, less strong as XB donor, colourless crystals formation occurred. The crystallographic structure analysis revealed they consisted of (HMTA)•Br_2 complexes.

The nitrogen atom of the Lewis base interacts through XB with the molecular bromine. This latter is the result of radical's reactions to which NBS molecule undergoes. After the cleavage of the covalent bond between the nitrogen and the bromine in the NBS molecule, free bromine radicals reacted together to form the correspondent molecular form.

Dihalogens can act as XB donors and, so, tend to form short contact interactions with the relative acceptor molecules. Indeed the distance between the positively charged bromine and the most nucleophilic nitrogen of HMTA results 2.088 Å, 38.8% less than the sum of their vdW radii.[91] The short and strong XB induces an elongation of the covalently bound bromines (Fig. 28a and b). Furthermore, the high strength of the XB is reflected by its high directionality. The angle formed between the nitrogen atom and the bromines is almost linear (175.25°).

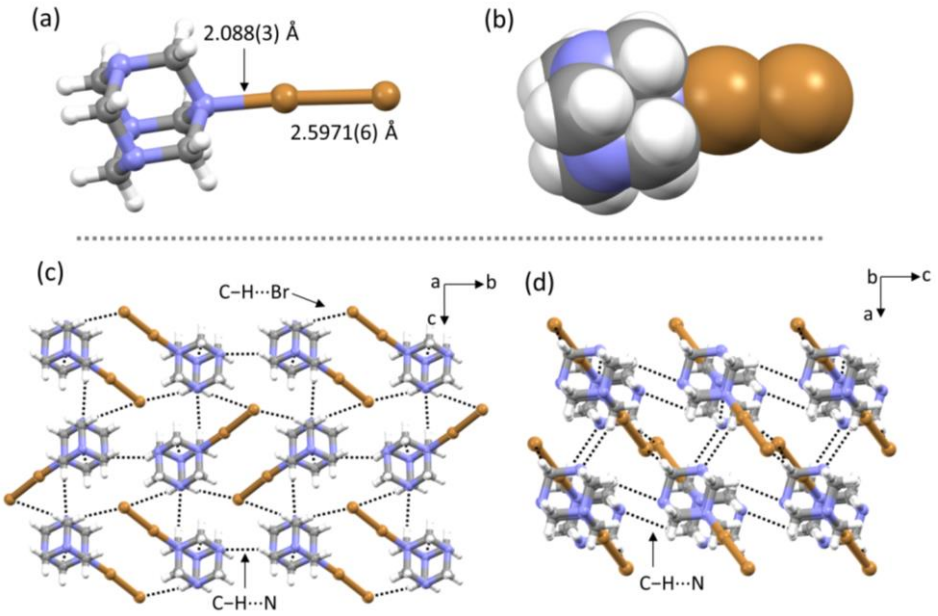

Figure 28 - A view of the structure (HMTA)•$(Br)_2$ with the distances of the halogen bonds (a), the relative CPK representation (b) and the crystal packing along the a-axis (c) and the b-axis (d).

The crystal structure analysis revealed that crystal packing is caused by hydrogen bonding forces. The nucleophilic bromine of the dihalogen alongside its electron density cloud interacts with

the –C-H moieties of adjacent HMTA molecules. Parallel, the free nitrogens in HMTA molecules (not participating on XBs' formation) exercise their electron withdrawal action to the –CH groups of adjacent HMTA molecules (Fig. 28c and d).

Even if the XB acceptor molecule, HMTA, is tetrafunctional, in terms of energy (HMTA)•Br_2 adducts are more stable.

3.3 Structure (HMTA)•2(C_6F_5I)

The trials performed with HMTA and NBS gave a complex where a molecular bromine interacts just with one nitrogen atom of HMTA. In a first step, thus, the attention of the work was turned to the analysis of the nucleophilicity of the Lewis base.

In this perspective, new XB donors were used to test HMTA nucleophilicity. Generally, strongly electronegative perfluoroalkyl residues further enhance the Lewis acid character (electron accepting ability) of halogen atoms in perfluorocarbon halides.[92] This fact led to choose iodopentafluorobenzene (C_6F_5I) and make it react with the tetrafunctional HMTA. Its benzene ring withdraws the electron density cloud of the iodine atom, and the electropositive σ-hole is intensified. As some studies reveal, the presence of fluorine atoms increases both the magnitude and the size of the σ-hole on iodine.[93]

Figures 29a and b show the dimers formed through XB interactions between the Iodine atoms and two of the four nitrogen atoms. Both contacts are short with R1=21.5% and R2=20.7% less than the sum of the vdW radii of the iodine and nitrogen atoms.[91] As shown, the distances of the two moieties are different meaning that one bonding is formed before the second one. This fact relies on the polarizability of the nitrogen atoms. The first nucleophile site is enough polarized to form a short contact distance with the iodine. Although less electronegative, the second nitrogen is again enough polarized to create a new bond with the other iodine but less strong than the first one. The resulting contact lengths are different.

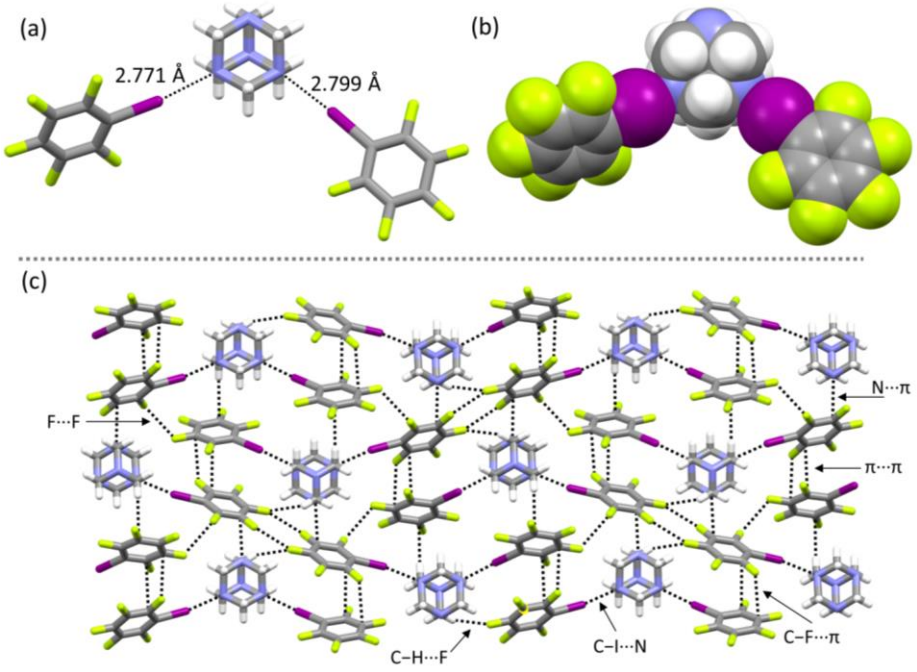

Figure 29 - A view of the structure (HMTA)•2(C_6F_5I) with the distances of the halogen bonds (a), the relative CPK representation (b) and the packing of the crystal structure (c).

In Figure 29c is evident that XB, HB, π interactions participate in the packing of the crystal. Interestingly, the electronegative fluorine shows its amphoteric character, interacting through its restricted σ-hole with the electron-rich lateral side of other fluorine atoms.

The nucleophilic character of HMTA was tested, and by the obtained results, just two nitrogen atoms are able to interact through XB.

In the following paragraphs, we will describe more experiments performed to verify again the nucleophilic character of the XB acceptor.

3.4 Structure (HMTA)•2(I_2)

The crystal structure of Figure 30a shows an HMTA molecule surrounded by two I_2. The N---I distances are shorter than those obtained with C_6F_5I (2.474 Å and 2.485 Å). This fact is reliable on the steric hindrance caused by the bigger C_6F_5I molecules.

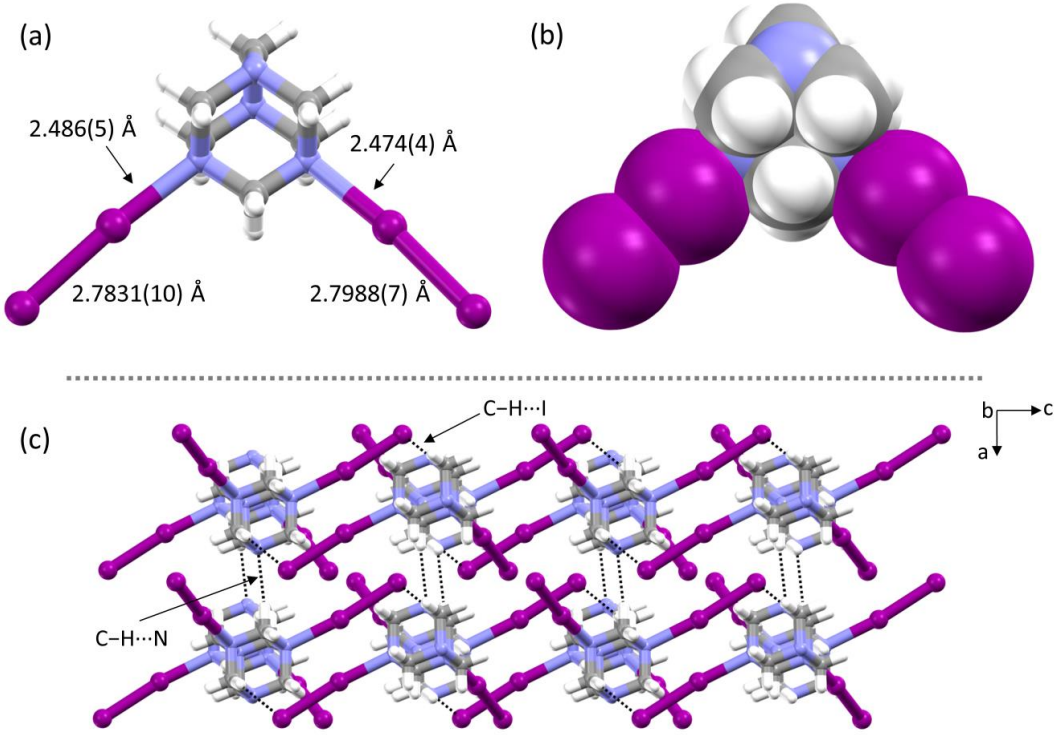

Figure 30 - A view of the structure (HMTA)•2I_2 with the distances between iodine and nitrogen atoms and the elongation of the molecular iodine (a), the relative CPK representation (b) and the crystal packing along the crystallographic axis b (c).

Even in this case, the interaction of the synthons occurred just with two nitrogen atoms. The different contact distance of the two XBs witnesses the interaction are formed at different times.

The crystal structure (Fig. 30c) reveals the presence of hydrogen bridges among the synthons. More specifically the -CH moieties of Lewis base interact with the free nitrogens of adjacent HMTA molecules and with the electronegative iodine. Chains that interlink and stack in a dislocated

manner to optimize the dispersion interactions between the iodines and the CH groups form the crystal packing.

3.5 Structure (HMTA)•2(BrCl)

More trials led to combine HMTA simultaneously with the strong XB donor NBS and with the weak XB donor NCS.

The crystal product is represented in Figure 31. Neither NBS nor NCS participated in the complexation of the structure. The chlorine atom provided by the NCS is attached to the bromine atom from the NBS molecule.

The bromine atoms interact with two nitrogen atoms on HMTA molecule. The intensified electropositive potential of bromine comes from the withdrawal effect of the electronegative chlorine atom. Generally, in dihalogen molecules, the activation of the halogen participating in a halogen bond increases with the decreasing atomic number of the second halogen.[93]

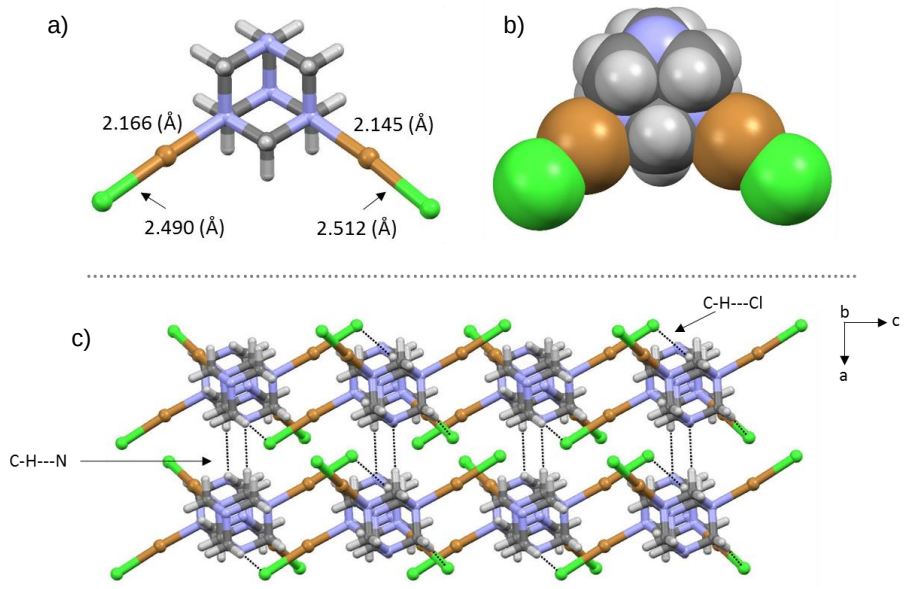

Figure 31 - A view of the structure (HMTA)•2(BrCl) with the distances between bromine and nitrogen atoms (a), the relative CPK representation (b) and the packing of the crystal structure (c).

Both contact distances are short (2.166 Å and 2.145 Å), 36.29% and 36.91% less than the sum of the vdW[91] radii. Due to polarization effect on the Lewis base, the XB cannot be formed

simultaneously, and the contact distances result with different lengths. Consequently, the elongation of the Cl-Br bond is different, as Figure 31a shows.

The electronegative side on chlorine atom interacts with the C-H groups of HMTA molecules in adjacent synthons, forming linear columns. These interlink one with another through hydrogen bonds between C-H groups of HMTA and the free nitrogen atoms in adjacent HMTA molecules (Fig. 31c).

3.6 Structure (HMTA)•2(ICl)

In the prospective to obtain the final crystalline structure of (HMTA)•4(NIS), HMTA, NIS and NCS were combined together. The crystallization solvent used was again the aprotic polar ACN. The results were similar to those achieved with NBS, in structure 3.5.

Figure 32 shows the final crystal structure obtained by the slow evaporation process. The contact distances of the XBs are 2.328 Å and 2.360 Å respectively, 34.05% and 33.14% less the sum of their vdW radii.[91]

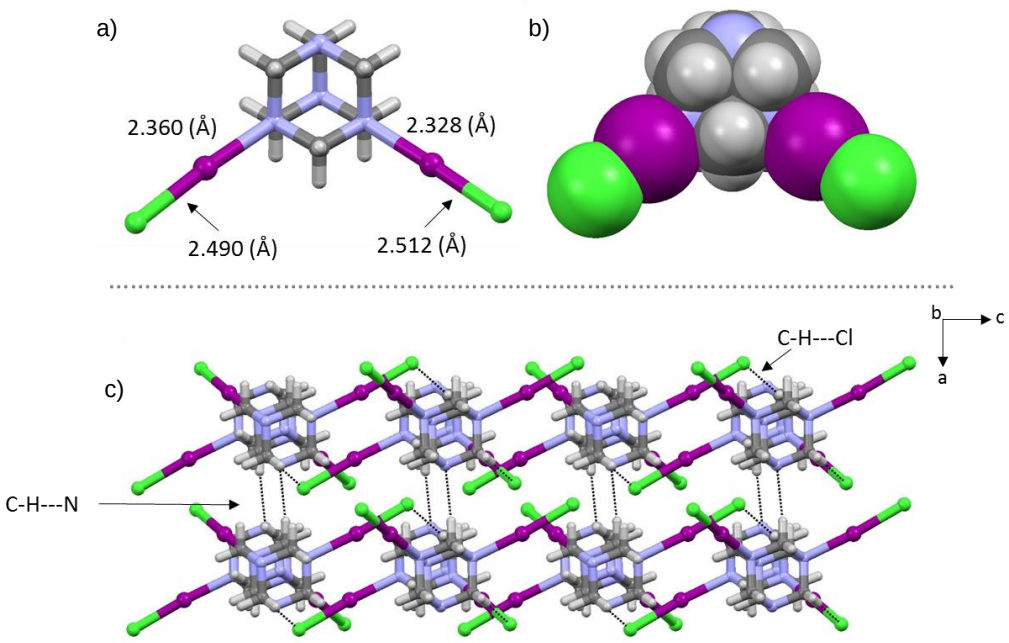

Figure 32 - A view of the structure (HMTA)•2(ICl) with the distances between iodine and nitrogen atoms (a), the relative CPK representation (b) and the packing of the crystal structure (c).

As most of the previous complexes, the different length between both distances indicated the fact they are not formed simultaneously. The nitrogen atom exercises a withdrawal action on the iodine causing the elongation of the covalent bond with the chlorine.

In the crystal packing (Fig. 32c), the motifs interlink and stack in chains through hydrogen bonds between the -CH moieties, the nitrogens, and the chlorines of adjacent XB acceptor molecules.

3.7 Structure (HMTA)•2(NBP)

N-bromophthalimide (NBP) molecule possesses an intensified electropositive potential along the covalent bond N-Br due to the higher withdrawal effect of the benzene ring.

The dropwise addition of NBP solution to the HMTA led to the precipitation of colourless crystalline blocks from a non-homogeneous solution, with a crystal structure belonging to the orthorhombic space group $Pmn2_1$ (Fig. 33).

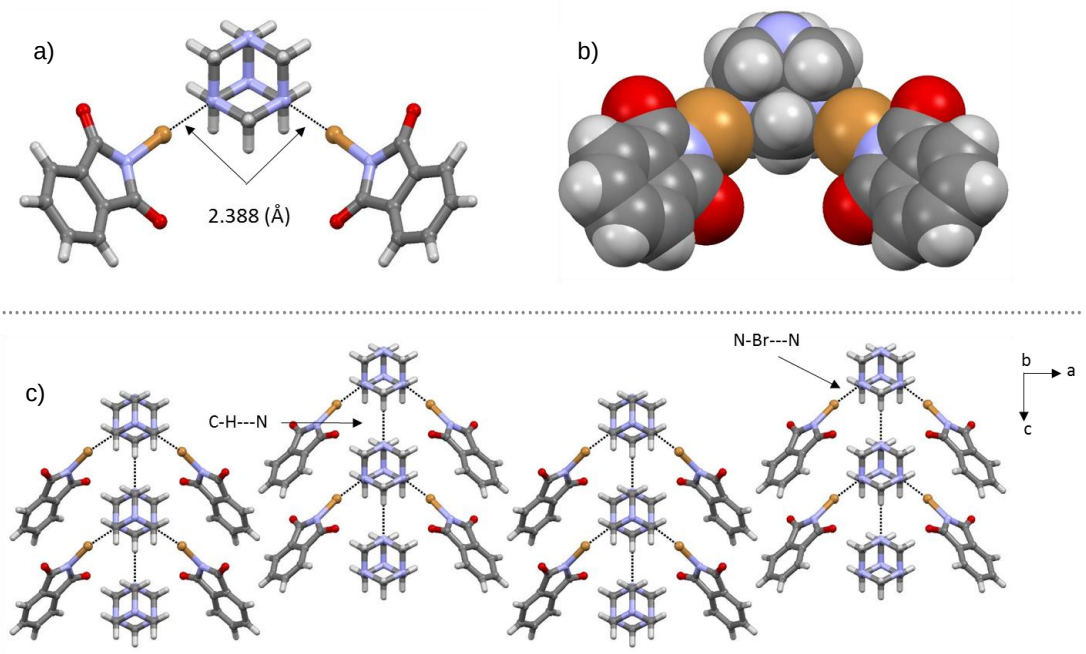

Figure 33 - A view of the structure (HMTA)•2(NBP) with the distances between the bromine and the two nucleophilic sites of HMTA (a), the relative CPK representation (b) and the relative crystal packing (c).

The crystallographic analysis revealed the formation of linear chains formed through hydrogen bonds between the -CH moieties and one of the nitrogen atoms of the HMTA molecule. Due to steric hindrance effects, the arrangement of the chains results in alternatively parallel rows. Differently, from all the previous listed structures, both XB distances are 2.388 Å, 29.76% less than the sum of their vdW radii (Fig. 33a and b).[91] Nevertheless, the polarization energy did not lead to the formation of the tetracoordinated complex.

The angle formed between the NBP molecule and the HMTA one is not as linear as expected (172.25°). Even if the bond strength is high, the steric hindrance of NBP molecule makes the XB donors assume a small angle alongside the noncovalent bond.

3.8 Structure (HMTA)•2(NBS)

The solvate crystal structure shown in Figure 34 recalls the reported one in 2013 by Raatikainen *et al.*[62]

The complex was obtained by adding neat NBS directly to a solution of HMTA in chloroform. This strategy aimed to avoid the cleavage of the covalently bound bromine-nitrogen atoms. In fact, N-bromosuccinimide is known to be a reagent employed mostly in free radical allylic and benzylic brominations, and for the electrophilic substitution of aromatic rings.[94] The addition of solid NBS to a solution of HMTA increases the probability to have a direct interaction between the Lewis acid and the Lewis base.

As expected, Figures 34a and b show two NBS molecules attached to one HMTA molecule. Differently from the N-bromophthalimide case, contact distances result to be not of the same length, 2.427 Å and 2.398 Å, 28.62% and 29.47% less than the sum of their vdW radii.[91]

In the crystallization process, the choice of the solvent played a key role. Chloroform is a halogenated solvent containing hydrogen atoms, thus, halogen bonding and hydrogen bonding co-exist.[95] Moreover, solvation had a significant influence on halogen bonding.[83] As the structure analysis shows, the framework contains chloroform molecules (Fig. 34c). They act as templates.

The acidic CH groups and the negative chlorines induced the dimeric complexation of the ligands. The formed dimers are interconnected through hydrogen bonds between the negative $C=O^-$ of NBS and the acidic C-H groups of HMTA.

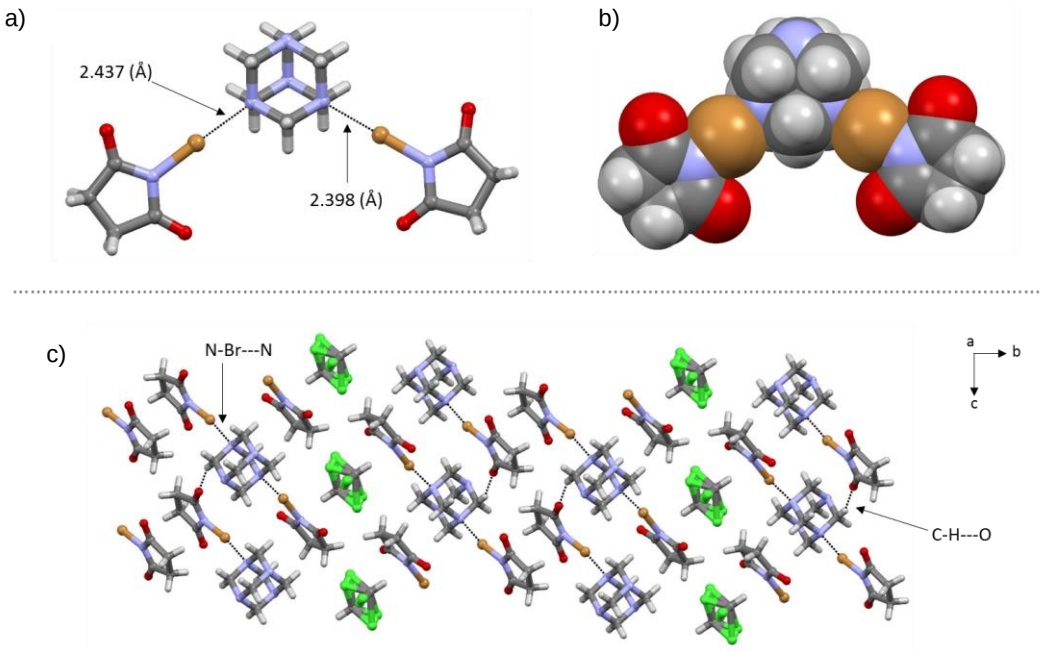

Figure 34 - A view of the structure (HMTA)•2(NBS) with the distances between the bromine and the two nucleophilic sites of HMTA (a), the relative CPK representation (b) and the crystal packing with the solvent molecules inclusion (c).

Even if the use of chloroform led to the complexation of the dimer, the resulting bulk system presents both the crystal precipitates and other white powder precipitates resulting a non-homogenous system.

3.9 Structure (HMTA)•4(NBS) @CH_2Cl_2

A particular porous structure was obtained by diluting HMTA and NBS after being ground together in DCM. The complex corresponds to three molecules of NBS interacting with the nucleophilic sites of the HMTA through XBs. Even if the contact distances are different for the three interactions, all of them result remarkably short (Fig. 35). The shorter bond (2.371 Å) was firstly

formed. This fact induced a depolarization of the rest part of the HMTA molecule. Consequently, the second XB results stronger than the third one (2.378 Å and 2.411 Å respectively).

As expected for an n to σ interaction,[96] also in this case, the halogen bond is directional. The angle between the covalent and noncovalent bonds is approximately of 180° confirming that the XB is preferentially along the axis of the orbital containing the lone pair of the electron donor. Moreover the shorter the interactions, the more directional they are. Indeed, as the lengths of the three bonds increase, the relative angles decrease from 177.90° of the shorter bond to 175.37°of the longer one.

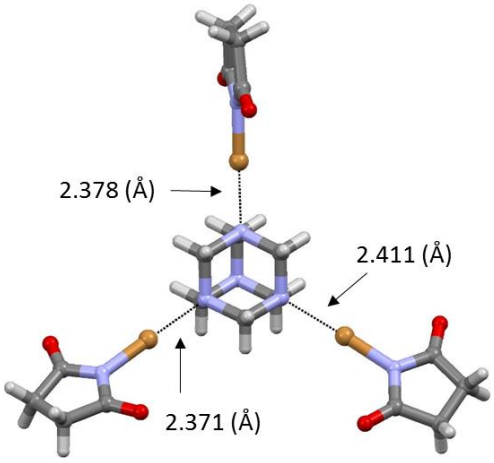

Figure 35 - A front view of the structure (HMTA)•4(NBS) with the distances between the three bromine atoms and the nucleophilic nitrogens of the HMTA molecule.

Figure 36 describes the CPK representations of the complex. The figure on the left shows the nucleophilic-electrophilic interaction between the carbonyl group of the XB donor and the electron-rich nitrogen atom of HMTA.

The crystal structure reveals the hydrogen bonding presence both between the acidic CH_2 groups of the HMTA with the OC^- of the NBS molecules, and between the OC^- with the acidic CH_2 of adjacent NBS molecules (fig. 37b). The competition between XBs and HBs led to the self-assembly of a porous structure. Figure 37 shows one-dimensional channels with a diameter of 10.147 Å X 8.206 Å occluding DCM molecules.

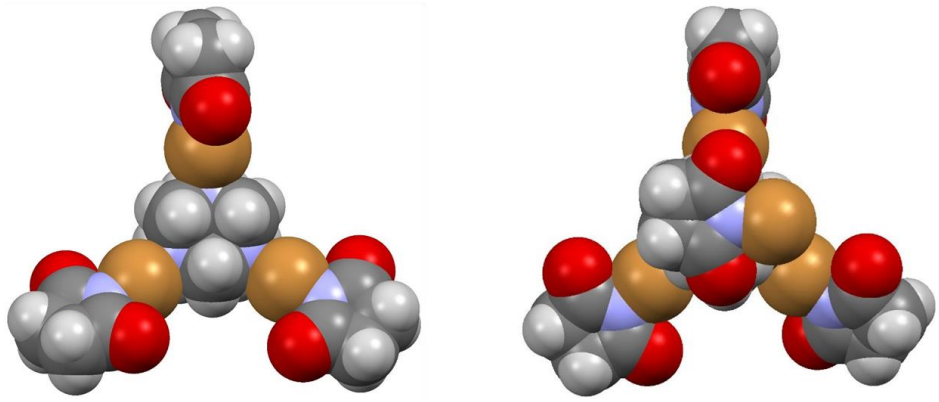

a) b)

Figure 36 - A front (a) and back (b) view of the structure (HMTA)•4(NBS) by CPK representation.

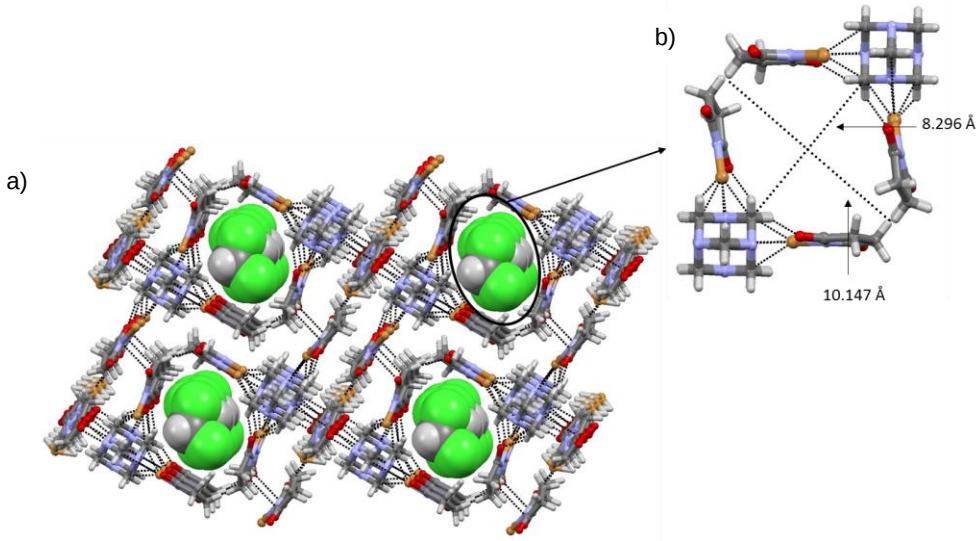

Figure 37 - A view of the crystal packing with the inclusion of the solvent molecules (a) and the diameters of the nanosized pores (b).

These channels occupy a volume of 200.8 $Å^3$, 2 per cell, the 13.4 % of the unit cell. This means that the voids encompass a small amount of the overall crystal space. The total surface to volume ratio is low, and the crystal structure in terms of porosity is not of good quality.

3.10 Structure (HMTA)•4(NBS) @CCl_4

The persistent studies of the behavior of the NBS molecule with the nucleophilic tetrafunctional HMTA led to the complexation of the (HMTA)•$(NBS)_4$ motif, solvated with tetrachloromethane molecules. The complex was obtained adopting the liquid-liquid diffusion crystallization technique.

The white interlayer formed after the addition of tetrachloromethane corresponded to a colloidal dispersion. Tetrachloromethane firstly induced a fast reaction and, then, due to the diffusion process, the system self-assembled around the solvent molecules and a host-channel system was formed (Fig. 38). The guest molecules adapted into the cavity through the electrostatic interactions with the acidic protons of the NBS molecules. The channels occupy a volume of 934.3 $Å^3$/cell, the 41.5 % of the unit cell.

The overall structure grew around the main motif (HMTA)•4(NBS) (Fig. 39), characterized by extremely short XB between the bromine and the nitrogen atoms, 2.401 Å, 29.38 % less than the sum of their vdW radii.[91] Differently, from the previous structures, all four-contact distances are of the same length. The polarization strength of the nucleophilic sites on the Lewis base, therefore, is equal. This fact is confirmed by the directionality of the four interactions. All four angles are almost linear, 179.33°, reflecting the high strength of the formed XBs.

As reported in Raatikainen *et al.*,[62] even if the complex is based on halogen interactions, the structure' skeleton is built up through those of hydrogen type. Figure 38c puts on evidence the hydrogen interactions between the acidic CH_2 groups of the HMTA molecule and the $C=O^-$ groups of the NBS one.

Further studies have to be developed in order to test the stability of the pores by changing the guest molecules. The coexistence of these crystal precipitates with others in the bulk prevents the calculations of the crystals yield from solution.

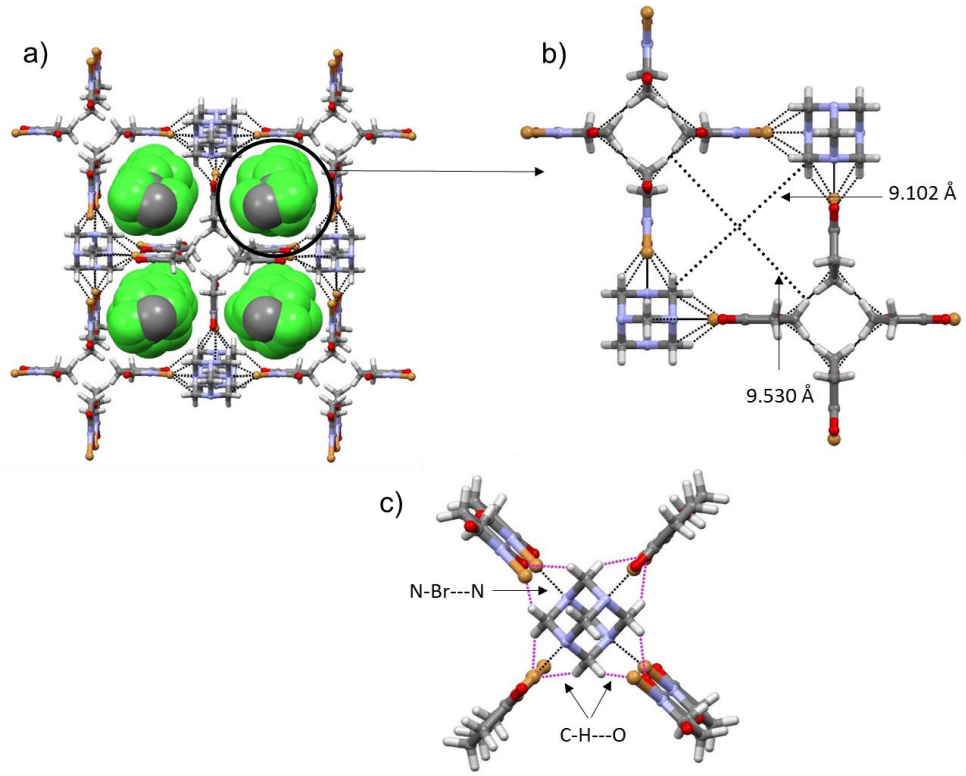

Figure 38 - A view of the crystal packing and the solvent inclusion (a); the dimeters of the nanosized pores (b) and the interactions (pink lines) between the adjacent complexes (c).

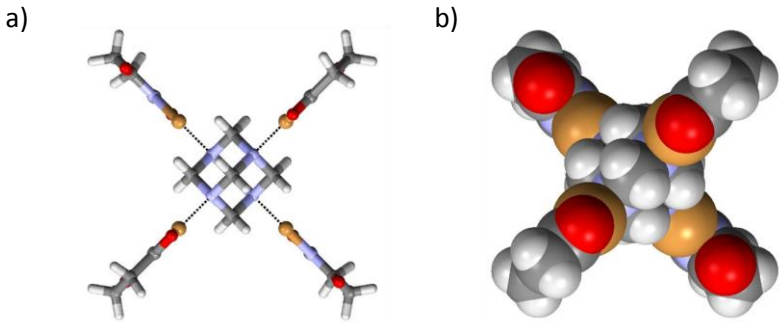

Figure 39 - A view of the structure (HMTA)•4(NBS) with the distances between the bromine and the nucleophilic sites of HMTA (2.401 Å) (a) and the relative CPK representation (b).

3.11 Structure (HMTA)•2(NIS)

This structure was obtained by the combination of several crystallization techniques. Firstly, the NIS molecule in a solution of DCM was slowly added to a solution of HMTA in chloroform, forming two separates layers with an interface. The separation was remarked by the instant formation of white colloids. Just after one day, crystalline colourless needles appeared but they re-dissolved into a solution that turned from colourless to a violet strong colour.

The instant formation of colloids occurred because nucleation took place at a high degree of supersaturation, so that the volume growth proceeds too quickly.[75] Consequently, a third layer was introduced in the interface between the two solutions to slow down the nucleation process. The HMTA solution was covered by the aprotic ACN, which acted as a diffusion chamber. Thus, NIS solution was added. After three days, thin crystalline plates precipitated from solution. The experiment was reproduced changing the crystallization solvents combination. Instead of solubilizing the ligands in apolar solvents, both of them were solubilized in ACN. The interlayer between the two solutions corresponded to a les polar solvent, such as chloroform, DCM, tetrachloromethane and toluene. The results were the same, thin crystalline plates were obtained.

Figure 40 presents the motif of the crystal. The contact distances of both halogen interaction are the same, 2.465 Å. They result 30.17% shorter than the sum of their vdW radii.[91]

Even in this case, the system did not present just one type of precipitates. This inhomogeneity affects the yield, and just a small amount of crystalline precipitates was possible to obtain.

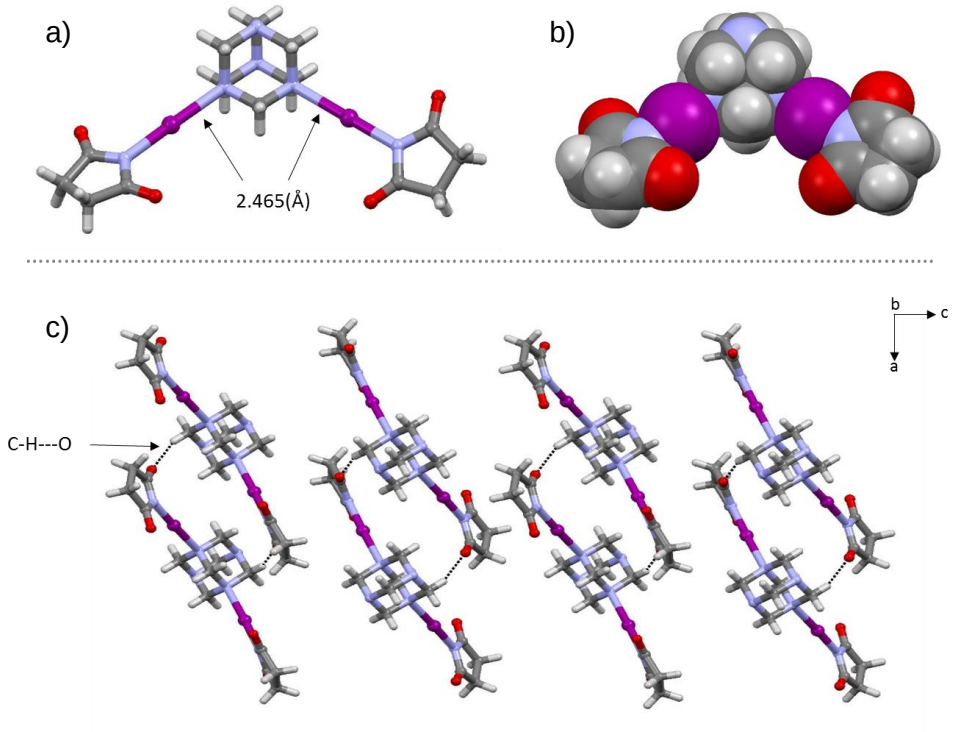

Figure 40 - A view of the structure (HMTA)•2(NIS) with the distances between the iodine and the two nucleophilic sites of HMTA (a), the relative CPK representation (b) and crystal packing (c).

3.12 Structure (HMTA)•4(NIS)

Figure 41 shows the complex formed by grinding HMTA together with molecular iodine and NCS. The final framework recalls the one reported by Raatikainen et al.[49,62]

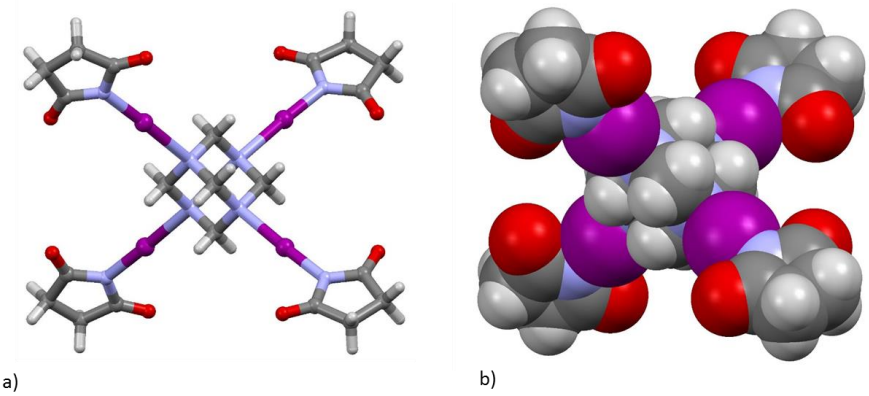

Figure 41 - A view of the structure (HMTA)•4(NIS) with the N-I---N distances of 2.501 Å (a) and the relative CPK representation (b).

Each distance between the iodine and the nitrogen atoms belonging to HMTA is remarkably short, 2.501 Å, which is about 29.15% shorter than the sum of their vdW radii.[91] The angle of the bond, 177.79°, is almost linear confirming again the strong nature of the interaction.

This stable supramolecular ribbon results when the self-complementary complexes stack and interlink via multiple H-bonds from acidic CH_2 groups of the HMTA molecule to C=O groups of the adjacent NIS moieties (Fig. 42).[49]

The adducts are assembled parallel forming a porous structure, where the channels occupy a volume of 949.1 $Å^3$, four per cell, the 40.6% of the unit cell. The acidic CH_2 groups of the HMTA favour the adaptation of DCM guest molecules into the cavities. The stability of the channels, thus, results reinforced by the templating effect of the solvent molecules.

As already shown, the crystal was obtained dissolving the ground neat starting materials in DCM. This fact implies that scheme 12 does not represent completely the reaction that led to the formation of this complex. The initial compounds, HMTA, NCS, and I_2, have already reacted in the mortar under the pestle action. A single crystal X-ray analysis cannot furnish the crystal structure of the powder material. Methodology for structure determination of molecular solids from powder X-ray diffraction data can be applied to establish the effectiveness of the new solid phase.[31] For technical reasons, powder X-Ray was not performed.

Both NCS and I_2 are compound used in radical and electrophilic reactions. When ground together, the probability to form radicals increases due to the pressure applied by the mortar action. Once in solution, the molecular recognition induces the self-assembling forming, thus, the complex (HMTA)•4(NIS). The precipitation of the crystal occurred once the solution was oversaturated and the colourless needles started to grow. Nevertheless, the inhomogeneity of the bulk system prevented the calculation of the yield. The use of chloroform instead of DCM led to twin crystals, not good enough for a single crystal X-ray analysis.

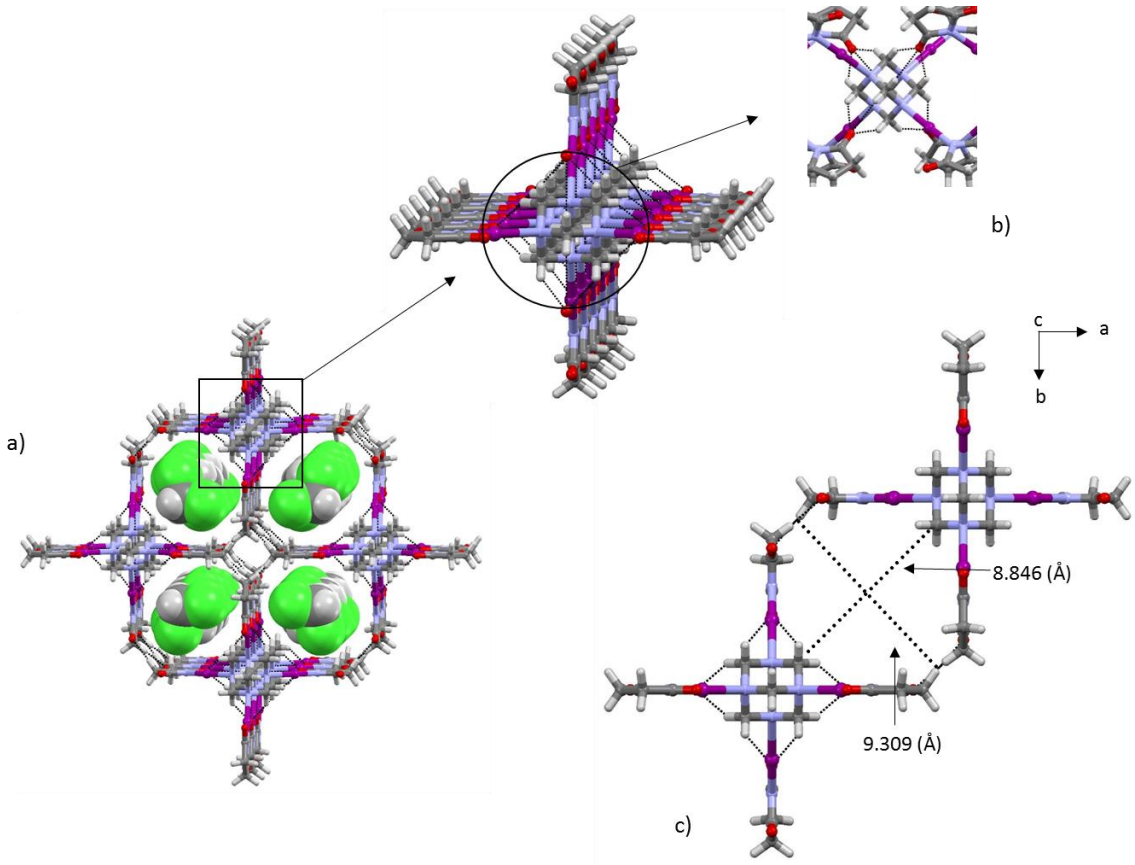

Figure 42 - A view of the crystal packing and the solvent inclusion (a); the interactions between hydrogen atoms and CO^- groups of the NIS moieties (b) and the diameters of the nanosized pores (c).

4. Conclusions

The present study gives an overview of several molecular crystal structures obtained by the combination of hexamethylenetetramine (HMTA) with different halogen bond donors. The nucleophilic character of the XB acceptor is affected both by the type of the halogen bond donor and by the experimental conditions.

The first crystalline structures were obtained by simply mixing solutions and leaving them under either vapor diffusion or slow evaporation at room temperature. The results have shown mostly motifs with XB characterized by short contact distances; nevertheless, in most of the cases, the complexation of the structure is due to hydrogen bonds and electrostatic interactions.

When neat NBS was added directly to a solution of HMTA in chloroform, the polarized bromines interacted with the four nitrogen atoms, forming the solvated structure of (HMTA)•4(NBS) with short contact distances. Parallel, the mixture of HMTA and NIS solutions through the layering technique led to the crystallization of stable dimers.

Mechanochemistry techniques maximized the electrophilic and nucleophilic interactions. In fact, by grinding HMTA molecules with weak and strong XB donors, such as NCS and molecular iodine, respectively, a solvated porous structure with stable 3D channels was obtained. The combination of mechanochemistry, with the traditional crystallization techniques, led to the final porous crystal structures.

Nonetheless, some practical factors influenced the results such as the inhomogeneity of the bulk system. Indeed, the quality of the crystals resulted proper for single crystal X-Ray analysis, but the amount obtained from solution was small.

In futures works, special attention should be given to the characterization of the participant ligands in the assembly of the final architecture throughout every step. X-Ray powder diffraction, nuclear magnetic resonance spectroscopy and single crystal X-Ray diffraction would suffice to characterize the ligands when in powder, in solution and in the final structure, single crystal.

References

(1) Lu, G. Q.; Zhao, X. S. (editors). *Nanoporous materials - an overview*; Nanoporous materials: Science and Engineering; Imperial College Press, U. K., 2004; Vol. 4, pp. 1-13.

(2) Fitzer, E.; Köchling, K.-H.; Boehm, H. P.; Marsh, H. Recommended terminology for the description of carbon as a solid (IUPAC Recommendations 1995). *Pure Appl. Chem.* **1995**. *67*, 473-506.

(3) Horie, K.; Barón, M.; Fox, R. B.; He, J.; Hess, M.; Kahovec, J.; Kitayama, T.; Kubisa, P.; Maréchal, E.; Mormann, W.; Stepto, R. F. T.; Tabak, D.; Vohlídal, J.; Wilks, E. S.; Work, W. J. Definitions of terms relating to reactions of polymers and to functional polymeric materials (IUPAC Recommendations 2003). *Pure Appl. Chem.* **2004**, *76*, 889–906.

(4) Sherman, D. J. Synthetic zeolites and other microporous oxide molecular sieves. *Proc. Natl. Acad. Sci.* **1999***, 96*, 3471-3478.

(5) Flanigen, E. M.; Broach, R. W.; Wilson, S. T. In: Zeolites in Industrial Separation and Catalysis. Kulprathipanja, S.; Wiley-VCH, Weinheim, 2001; pp. 1-26.

(6) Na, K.; Somorjai, G.A. Hierarchically Nanoporous Zeolites and Their Heterogeneous Catalysis: Current Status and Future Perspectives. *Catal Lett.* **2015**, *145*, 193–213.

(7) Auerbach, S. M.; Carrado, K. A.; Dutta, P. K. (editors). Handbook of Zeolite Science and Technology; Marcel Dekker, U.S., 2003; pp. 1.

(8) Jha, B.; Singh, D. N. Fly Ash Zeolites - Innovations, Applications, and Directions; Springer, Singapore, 2016; pp. 6.

(9) Jacobs, P.A.; Flanigen, E.M.; Jansen, J.C.; Bekkum, H.V. (editors). Introduction to Zeolite Science and Practice; Elsevier, Netherlands, 2001; pp. 39.

(10) Argauer, R.J.; Landolt, G.R. Crystalline zeolite ZSM-5 and method for preparing the same. U.S. Patent 3, 702.886, Nov 14th, 1972.

(11) Cundy, C. S.; Cox, P. A. The Hydrothermal Synthesis of Zeolites: History and Development from the Earliest Days to the Present Time. *Chem. Rev.* **2003**, *103*, 663−701.

(12) Cundy, C. S.; Zhao, J. P. Remarkable synergy between microwave heating and the addition of seed crystals in zeolite synthesis—a suggestion verified. *Chem. Commun.* **1998**, 1465-1466.

(13) Sang, S.; Chang, F.; Liu, Z.; He, C.; He, Y.; Xu, L. Difference of ZSM-5 zeolites synthesized with various templates. *Catal. Today*, **2004,** *93–95,* 729–734.

(14) Xu, W.; Dong, J.; Li, J.; Li, J; Wu, F. A Novel Method for the Preparation of Zeolite ZSM-5. *J. Chem. Soc., Chem. Commun.* **1990**, *0*, 755-756.

(15) Guisnet, M.; Gilson (editors), J.P. *Introduction to Zeolite Science and Technology;* Zeolites for Cleaner Technologies; Imperial College Press: London, 2001; Vol. 3, pp. 1-28.

(16) Yilmaz, B.; Müller, U. Catalytic Applications of Zeolites in Chemical Industry. *Top Catal.* **2009**, *52*, 888–895.

(17) Ennaert, T.; Van Aelst, J.; Dijkmans, J.; De Clercq, R.; Schutyser, W.; Dusselier, M.; Verboekend, D.; Sels, B.F. Potential and challenges of zeolite chemistry in the catalytic conversion of biomass. *Chem. Soc. Rev.* **2016***, 45*, 584-611.

(18) Wang, Y.; Tuel, A. Nanoporous zeolite single crystals: ZSM-5 nanoboxes with uniform intracrystalline hollow structures. *Microporous Mesoporous Mater.* **2008***, 113,* 286-295.

(19) Tosheva, L.; Valtchev, V.P. Nanozeolites: Synthesis, Crystallization Mechanism, and Applications. *Chem. Mater.* **2005***, 17*, 494-2513.

(20) Mitchell, S.; Pinar, A.B.; Kenvin, J.; Crivelli, P.; Kärger, J.; Pérez-Ramìrez, J. Structural analysis of hierarchically organized Zeolites. *Nat. Commun.* **2015,** *6,* 8633-8647.

(21) Dhakshinamoorthy, A.; Alvaro, M.; Corma, A.; Garcia, H. Delineating similarities and dissimilarities in the use of metal organic frameworks and zeolites as heterogeneous catalysts for organic reactions. *Dalton Trans.* **2011***, 40*, 6344-6360.

(22) Farrusseng, D.; Aguado, S.; Pinel, C. Metal–Organic Frameworks: Opportunities for Catalysis. *Angew. Chem. Int. Ed.* **2009***, 48*, 7502-7513.

(23) Furukawa, H.; Cordova, K. E.; O'Keeffe, M.; Yaghi, O. M. The Chemistry and Applications of Metal-Organic Frameworks. *Science,* **2013***, 341,* 974-988.

(24) Hong-Cai, Z.; Long, J. R.; Yaghi, O.M. Introduction to Metal−Organic Frameworks. *Chem. Rev.* **2012***, 112,* 673-673.

(25) Férey, G. Microporous Solids: From Organically Templated Inorganic Skeletons to Hybrid Frameworks...Ecumenism in Chemistry. *Chem. Mater.* **2001***, 13*, 3084-3098.

(26) Czaja, A. U.; Trukhan, N.; Müller, U. Industrial applications of metal–organic frameworks. *Chem. Soc. Rev.* **2009**, *38*, 1284–1293.

(27) Chui, S. S. Y.; Lo, S. M. F.; Charmant, J. P.; Orpen, A. G.; Williams, I. D. A chemically functionalizable nanoporous material [Cu3(TMA)2(H2O)3]. *Science*, **1999**, *283*, 1148–50.

(28) Keskin, S.; Kızılel, S. Biomedical Applications of Metal Organic Frameworks. *Ind. Eng. Chem. Res.* **2011**, *50*, 1799–1812.

(29) Li, H.; Eddaoudi, M.; O'Keeffe, M.; Yaghi, O.M. Design and synthesis of an exceptionally stable and highly porous metal-organic framework. *Nature,* **1999***, 402*, 276-279.

(30) Robson, R. Design and its limitations in the construction of bi- and poly-nuclear coordination complexes and coordination polymers (aka MOFs): a personal view, *Dalton Trans.* **2008**, *38*, 5113-5131.

(31) Hong-Cai, J.Z.; Kitagawa, S. Metal–Organic Frameworks (MOFs). *Chem. Soc. Rev.* **2014***, 43,* 5415-5418.

(32) Rowsell, J. L.C.; Yaghi, O. M. Metal–organic frameworks: a new class of porous materials, *Microporous Mesoporous Mater.* **2004**, *73,* 3-14.

(33) Shekhah, O.; Wang, H.; Zacher, D.; Fischer, R. A.; Wöll, C. Growth Mechanism of Metal–Organic Frameworks: Insights into the Nucleation by Employing a Step-by-Step Route. *Angew. Chem. Int. Ed*. **2009**, *48*, 5038 –5041.

(34) Keskin, S.; Sholl, D. S. Efficient Methods for Screening of Metal Organic Framework Membranes for Gas Separations Using Atomically Detailed Models. *Langmuir*, **2009**, *25,* 11786–11795.

(35) Perry, J. J.; Perman, J. A.; Zaworotko, M. J. Design and synthesis of metal–organic frameworks using metal–organic polyhedra as supramolecular building blocks. *Chem. Soc. Rev*. **2009**, *38*, 1400–1417.

(36) MOF-5 (or IRMOF-1) Metal Organic Framework. URL:<http://www.chemtube3d.com/solidstate/MOF-MOF5.html> (accessed on Aug 6th,.2017).

(37) Eddaoudi, M.; Kim, J.; Rosi, N.; Vodak, D.; Wachter, J.; O'Keeffe, M.; Yaghi, O. M. Systematic Design of Pore Size and Functionality in Isoreticular MOFs and Their Application in Methane Storage. *Science*, **2002**, *295*, 469-472.

(38) Zhou, D.D.; Xu, Y.T.; Lin, R.B.; Mo, Z.W.; Zhang, W.Z.; Zhang, J.P. High-symmetry hydrogen-bonded organic frameworks: air separation and crystal-to-crystal structural transformation. *Chem. Commun.* **2016**, *52*, 4991-4994.

(39) Metrangolo, P.; Resnati, G. (editors). *Halogen Bonding Fundamentals and Applications;* Springer, Berlin, 2008; pp. 8-9.

(40) Legon, A.C. The halogen bond: an interim perspective. *Phys. Chem. Chem. Phys.* **2010**, *12*, 7736–7747.

(41) Karpfen, A. Theoretical Characterization of the Trends in Halogen Bonding. *Struct. Bond.* **2008**, *126*, 1–15.

(42) Metrangolo, P.; Resnati, G. Halogen Bonding: A Paradigm in Supramolecular Chemistry. *Chem. Eur. J.* **2001**, *7* , 2511-2519.

(43) Pennington, W. T.; Hanks, T.W.; Arman, H.D. Halogen Bonding with Dihalogens and Interhalogens. *Struct. Bond.* **2008**, 126, 65-104.

(44) Brown, A.; Beer, P. D. Halogen bonding anion recognition. *Chem. Commun*. **2016**, *52*, 8645-8658.

(45) Awwadi, F. F.; Willett, R. D.; Peterson, K. A.; Twamley, B. The Nature of Halogen···Halogen Synthons: Crystallographic and Theoretical Studies. *Chem. Eur. J.* **2006**, *12*, 8952 – 8960.

(46) Metrangolo, P.; Resnati, G.; Pilati, T.; Biella, S. Halogen Bonding in Crystal Engineering. *Struct. Bond.* **2008**, 126, 105–136.

(47) Jia, J.; Lin, X.; Wilson, C.; Blake, A.J.; Champness, N.R.; Hubberstey, P.; Walker, G.; Cussena, E.J.; Schroder, M. Twelve-connected porous metal–organic frameworks with high H_2 adsorption, *Chem. Commun.* **2007**, 840-842.

(48) Vallet-Regi, M.; Balas, F.; Arcos, D. Mesoporous Materials for Drug Delivery. *Angew. Chem. Int. Ed.*, **2007**, *46*, 7548-7558.

(49) Raatikainen, K.; Rissanen, K. Breathing molecular crystals: halogen- and hydrogen-bonded porous molecular crystals with solvent induced adaptation of the nanosized channels. *Chem. Sci.* **2012**, *3*, 1235-1239.

(50) Cavallo, G.; Metrangolo, P.; Pilati, T.; Resnati, G.; Terraneo, G. Halogen Bond: A Long Overlooked Interaction. *Top. Curr. Chem.* **2015**, 358, 1–18.

(51) Hassel, O.; Hvoslef, J. The structure of bromine 1,4-dioxanate. *Acta Chem. Scand*. **1954**, 8, 873.

(52) Politzer, P.; Murray, J. S.; Clark, T. Halogen bonding and other σ-hole interactions: a perspective, *Phys.Chem. Chem. Phys.* **2013**, *15*, 11178-11189.

(53) Politzer, P.; Murray, J. S. The fundamental nature and role of the electrostatic potential in atoms and molecules. *Theor. Chem. Acc*. **2002**, *108,* 134–142.

(54) W. Bader, R. F.; Carroll, M. T.; Cheeseman, J. R.; Chang, C. Properties of atoms in molecules: atomic volumes. *J. Am. Chem. Soc*. **1987**, *109*, 7968–7979.

(55) Politzer, P.; Murray, J. S.; Clark, T. σ-Hole Bonding: A Physical Interpretation. *Top. Curr. Chem.* **2015**; Vol. 358, 19–42.

(56) Yunxiang, L.; Haiying, L.; Xiang, Z.; Weiliang, Z.; Honglai, L. How Does Halogen Bonding Behave in Solution? A Theoretical Study Using Implicit Solvation Model. *J. Phys. Chem. A*. **2011**, *115*, 4467–4475.

(57) Metrangolo, P.; Murray, J. S.; Pilati, T.; Politzer, P.; Resnati, J.; Terraneo, G. The fluorine atom as a halogen bond donor, viz. a positive site. *Cryst. Eng. Comm*. **2011**, *13*, 6593-6596.

(58) Goroff, N. S.; Curtis, S. M.; Webb, J. A.; Fowler, F. W.; Lauher, J. W. Designed Cocrystals Based on the Pyridine-Iodoalkyne Halogen Bond. *Org. Lett*. **2005**, *7*, 1891-1893.

(59) Aakeröy, C. B.; Baldrighi, M.; Desper, J.; Metrangolo, P.; Resnati, G. Supramolecular Hierarchy among Halogen-Bond Donors. *Chem. Eur. J*. **2013**, *19*, 16240 – 16247.

(60) Alkorta, I.; Rozas, I.; Elguero, J. Charge-Transfer Complexes between Dihalogen Compounds and Electron Donors**.** *J. Phys. Chem. A.* **1998***, 102,* 9278- 9285.

(61) Brown, R. N. The Crystal Structure of N-Chloro-Succinimide. *Acta Cryst.***1961**, *14*, 711-715.

(62) Raatikainen, K.; Rissanen, K. Interaction between amines and N-haloimides: a new motif for unprecedentedly short Br/N and I/N halogen bonds. *Cryst. Eng. Comm.* **2011**, *13,* 6972-6977.

(63) Troff, R. W.; Mäkelä, T.; Topić, F.; Valkonen, A.; Raatikainen, K.; Rissanen, K. Alternative Motifs for Halogen Bonding. *Eur. J. Org. Chem.* **2013**, 1617–1637.

(64) Ormond-Prout, J. E.; Smart, P.; Brammer, L. Cyanometallates as Halogen Bond Acceptors. *Cryst. Growth Des*. **2012**, *12*, 205−216.

(65) Amico, V.; Meille, S. V.; Corradi, E.; Messina, M. T; Resnati, R. Perfluorocarbon Hydrocarbon Self-Assembling. 1D Infinite Chain Formation Driven by Nitrogen---Iodine Interactions. *J. Am. Chem. Soc.* **1998,** *120,* 8261-8262.

(66) Peuronen, A.; Valkonen, A.; Kortelainen, M.; Rissanen, K.; Lahtinen, M. Halogen Bonding-Based “Catch and Release” Reversible Solid-State Entrapment of Elemental Iodine with Monoalkylated DABCO Salts. *Cryst. Growth Des*. **2012**, *12*, 4157−4169.

(67) Arunan, E.; Desiraju, G. R.; Klein, R. A.; Sadlej, J.; Scheiner, S.; Alkorta, I.; Clary, D. C.; Crabtree, R. H.; Dannenberg, J. J.; Hobza, P.; Kjaergaard, H. G.; Legon, A. C.; Mennucci, B.; Nesbitt, D. J. Definition of the hydrogen bond (IUPAC Recommendations 2011). *Pure Appl. Chem.* **2011***, 83*, 1637–1641.

(68) Primagi, A.; Cavallo, G.; Metrangolo, P.; Resnati, G. The Halogen Bond in the Design of Functional Supramolecular Materials: Recent Advances. *Accounts Chem. Res*. **2013**, *46,* 2686-2695.

(69) Lu, Y.; Wang, Y.; Zhu, W. Nonbonding interactions of organic halogens in biological systems: implications for drug discovery and biomolecular design. *Phys. Chem. Chem. Phys*. **2010**, *12*, 4543–4551.

(70) Aakeröy, C. B.; Spartz, C. L.; Dembowski, S.; Dwyre, S.; Desper., J. A systematic structural study of halogen bonding versus hydrogen bonding within competitive supramolecular systems. *IUCrJ,* **2015**, *2*, 498–510.

(71) Raatikainen, K.; Cametti, M.; Rissanen, K. The subtle balance of weak supramolecular interactions: The hierarchy of halogen and hydrogen bonds in haloanilinium and halopyridinium salts. *Beilstein J. Org. Chem*. **2010**, *6*, 1-13.

(72) Borchardt-Ott, W (editor). *The Crystalline State.* Crystallography - An Introduction, 3rd Edition; Springer, Berlin, 2012, pp. 3-8.

(73) Atomic Scale Structure of Materials. <https://www.doitpoms.ac.uk/tlplib/atomic-scale-structure/printall.php> (accessed on Aug 6th, 2017).

(74) Hulliger, J. Chemistry and Crystal Growth, *Angew. Chem. Int. Ed. Engl.* **1994,** *33*, 143-162.

(75) Massa, W. *Crystal structure determination,* 1st Edition; Springer, Berlin, 2000.

(76) Atkins, P.; De Paula, *J. Physical Chemistry*, 9Th Edition; W.H. Freeman and Company, New York, 2010.

(77) Amorós, J.L.; Buerger, M.J.; De Amorós, M.C. *The Laue Method.* Academic Press, USA, 1975.

(78) Seibert, J. A. X-Ray Imaging Physics for Nuclear Medicine Technologists. Part 1: Basic Principles of X-Ray Production. *J. Nucl. Med. Technol*. **2004**, *32*,139–147.

(79) Holden, A.; Morrison, P. *Crystals and Crystal Growing*. Singer, Anchor Books-Doubleday, New York, 1960.

(80) Carlucci, L.; Ciani, G.; Proserpio, D. M.; Sironi, A. A Novel 3D Three-Connected Cubic Network Containing [Ag6(hmt)6]6+ Hexagonal Units (hmt) Hexamethylenetetramine). *Inorg. Chem.* **1997***, 36,* 1736-1737*.*

(81) James, S. L.; Adams, C. J; Bolm, C.; Braga, D.; Collier, P.; Friščić, T.; Grepioni, F.; Harris, K. D. M.; Hyett, G.; Jones, W.; Krebs, A.; Mack, J.; Maini, L.; Orpen, A. G.; Parkin, I. P.; Shearouse, W. C.; Steed, J. W.; Waddell, D. C. Mechanochemistry: opportunities for new and cleaner synthesis. *Chem. Soc. Rev*. **2012**, *41*, 413–447.

(82) Lommerse, J. P. M.; Stone, A. J.; Taylor, R.; Allen, F. H. The Nature and Geometry of Intermolecular Interactions between Halogens and Oxygen or Nitrogen. *J. Am. Chem. Soc.* **1996,** *118,* 3108-3116.

(83) Carlsson, A. C. C.; Veiga, A. X.; Erdélyi, M. Halogen Bonding in Solution. *Top.Curr.Chem*. **2015**, *359,* 49–76.

(84) Rigaku Oxford Diffraction 2015, *CrysAlisPro* version 38.43.

(85) Bruker AXS BV*, Madison, WI, USA;* 1997–2004.

(86) Otwinowski, Z.; Minor, W. Processing of X-ray diffraction data collected in oscillation mode. *Methods Enzymol.* **1997**, *276*, 307–326.

(87) Blessing, R. H. Outlier Treatment in Data Merging. *Appl. Cryst.* **1997**, *30*, 421–426.
(88) Sheldrick, G.M. Crystal structure refinement with SHELXL. *Acta Cryst. A*. **2015**, *71*, 3-8.
(89) Dolomanov, O. V.; Bourhis, L. J.; Gildea, R. J.; Howard, J. A. K.; Puschmann. H. OLEX2: a complete structure solution, refinement and analysis program. *Appl. Cryst.* **2009**, *42*, 339-341.

(90) Metrangolo, P.; Neukirch, H.; Pilati, T.; Resnati, G. Halogen Bonding Based Recognition Processes: A World Parallel to Hydrogen Bonding. *Acc. Chem. Res.* **2005***, 38,* 386-395.
(91) Bondi, A. Van der Waals Volumes and Radii. *J. Phys. Chem.* **1964**, *68*, 41-51.

(92) Wasilewska, A; Gdaniec, M.; Polonski, T. Co-crystals of iodopentafluorobenzene with nitrogen donors: 2-D molecular assemblies through halogen bonding and aryl–perfluoroaryl interactions. *Cryst. Eng. Comm.* **2007***, 9,* 203-206.
(93) Kolář, M.H.; Deepa, P.; Ajani, H.; Pecina, A.; Hobza, P. Characteristics of a σ-Hole and the Nature of a Halogen Bond. *Top. Curr. Chem.* **2015**, 359, 1-26.
(94) Carreno, M. C.; Garcia Ruano, J. L.; Sanz, G.; Toledo, M.A.; Urbano, A. N-Bromosuccinimide in Acetonitrile: A Mild and Regiospecific Nuclear Brominating Reagent for Methoxybenzenes and Naphthalenes. *J. Org. Chem*. **1995**, *60*, 5328-5331.
(95) Xue, P.; Jin, W.J. Exploring the halogen bond specific solvent effects in halogenated solvent systems by ESR probe. *New J.Chem.* **2015**, *39*, 5477—5483.
(96) Forni, A.; Metrangolo, P.; Pilati, T., Resnati, G. Halogen Bond Distance as a Function of Temperature, *Crystal Growth & Design.* **2004***, 4,* 291-295.

Annexes

Table 7– List of XB contact distances with the relative R values.

	d_{N---Br} (Å)	d_{N---I} (Å)	R (%)*
Structure 2	2.088		0.388
Structure 3		2.771 2.799	0.215 0.207
Structure 4		2.474 2.486	0.299 0.260
Structure 5	2.145 2.166		0.363 0.369
Structure 6		2.328 2.360	0.341 0.331
Structure 7	2.388		0.298
Structure 8	2.398 2.437		0.295 0.286
Structure 9	2.371 2.378 2.411		0.302 0.300 0.294
Structure 10	2.401		0.294
Structure 11		2.465	0.302
Structure 12		2.501	0.292

*R values calculated according the equation 4.

Table 8 - Crystal data and structure refinement for $(HMTA^{-}CH_2OH)^{+}Cl^{-}$.

Empirical formula	$C_7H_{15}ClN_4O$
Formula weight	206.68
Temperature/K	170.0(1)
Crystal system	Monoclinic
Space group	$P2_1/n$
a/Å	6.2647(13)
b/Å	10.222(2)
c/Å	14.713(3)
α/°	90
β/°	97.06(3)
γ/°	90
Volume/Å^3	935.0(3)
Z	4
ρ_{calc} *g/cm^3*	1.468
μ/mm^{-1}	0.376
F(000)	440.0
Crystal size/mm^3	0.11 × 0.1 × 0.1
Radiation	MoKα (λ = 0.71073)
2Θ range for data collection/°	4.864 to 50.49
Index ranges	-7 ≤ h ≤ 7, -12 ≤ k ≤ 10, -17 ≤ l ≤ 17
Reflections collected	6113
Independent reflections	1700 [R_{int} = 0.0524, R_{sigma} = 0.0611]
Data/restraints/parameters	1700/0/119
Goodness-of-fit on F^2	1.035
Final R indexes [I>=2σ (I)]	R_1 = 0.0439, wR_2 = 0.0864
Final R indexes [all data]	R_1 = 0.0708, wR_2 = 0.0962
Largest diff. peak/hole / e Å^{-3}	0.26/-0.21

Table 9 - Crystal data and structure refinement for (HMTA) (Br2).

Empirical formula	$C_6H_{12}Br_2N_4$
Formula weight	300.02
Temperature/K	120.0(1)
Crystal system	Monoclinic
Space group	$P2_1/c$
a/Å	5.9077(2)
b/Å	13.7052(4)
c/Å	11.8940(4)
α/°	90
β/°	99.273(3)
γ/°	90
Volume/Å³	950.43(5)
Z	4
ρ_{calc} *g/cm³*	2.097
μ/mm⁻¹	8.482
F(000)	584.0
Crystal size/mm³	0.4 × 0.272 × 0.093
Radiation	MoKα (λ = 0.71073)
2Θ range for data collection/°	6.886 to 50.496
Index ranges	-6 ≤ h ≤ 7, -15 ≤ k ≤ 16, -14 ≤ l ≤ 10
Reflections collected	4698
Independent reflections	1717 [R_{int} = 0.0456, R_{sigma} = 0.0508]
Data/restraints/parameters	1717/0/109
Goodness-of-fit on F²	1.083
Final R indexes [I>=2σ (I)]	R_1 = 0.0328, wR_2 = 0.0761
Final R indexes [all data]	R_1 = 0.0385, wR_2 = 0.0787
Largest diff. peak/hole / e Å⁻³	0.51/-0.71

Table 10 - Crystal data and structure refinement for (HMTA) 2(C_6F_5I).

Empirical formula	$C_{18}H_{12}F_{10}I_2N_4$
Formula weight	728.12
Temperature/K	120.0(1)
Crystal system	Monoclinic
Space group	$P2_1/c$
a/Å	5.97390(10)
b/Å	14.6245(4)
c/Å	24.7926(6)
α/°	90
β/°	90.905(2)
γ/°	90
Volume/Å^3	2165.74(9)
Z	4
ρ_{calc}g/cm^3	2.233
μ/mm^{-1}	3.005
F(000)	1376.0
Crystal size/mm^3	0.163 × 0.136 × 0.116
Radiation	MoKα (λ = 0.71073)
2Θ range for data collection/°	5.808 to 50.488
Index ranges	-7 ≤ h ≤ 7, -17 ≤ k ≤ 17, -29 ≤ l ≤ 29
Reflections collected	14770
Independent reflections	3912 [R_{int} = 0.0329, R_{sigma} = 0.0308]
Data/restraints/parameters	3912/0/307
Goodness-of-fit on F^2	1.041
Final R indexes [I>=2σ (I)]	R_1 = 0.0227, wR_2 = 0.0434
Final R indexes [all data]	R_1 = 0.0278, wR_2 = 0.0459
Largest diff. peak/hole / e Å^{-3}	0.39/-0.38

Table 11 - Crystal data and structure refinement for (HMTA) 2(I2).

Empirical formula	$C_6H_{12}I_4N_4$
Formula weight	647.80
Temperature/K	170.0(1)
Crystal system	Monoclinic
Space group	$P2_1/c$
a/Å	6.0836(12)
b/Å	16.606(3)
c/Å	14.709(3)
α/°	90
β/°	92.12(3)
γ/°	90
Volume/Å³	1484.9(5)
Z	4
ρ_{calc} *g/cm³*	2.898
μ/mm⁻¹	8.371
F(000)	1152.0
Crystal size/mm³	0.17 × 0.13 × 0.13
Radiation	MoKα (λ = 0.71073)
2Θ range for data collection/°	3.7 to 50.496
Index ranges	$-7 \le h \le 7$, $-19 \le k \le 19$, $-15 \le l \le 17$
Reflections collected	9999
Independent reflections	2692 [R_{int} = 0.0404, R_{sigma} = 0.0419]
Data/restraints/parameters	2692/0/127
Goodness-of-fit on F²	1.045
Final R indexes [I>=2σ (I)]	R_1 = 0.0305, wR_2 = 0.0548
Final R indexes [all data]	R_1 = 0.0400, wR_2 = 0.0574
Largest diff. peak/hole / e Å⁻³	0.64/-0.77

Table 12 - Crystal data and structure refinement for (HMTA) 2(BrCl).

Empirical formula	$C_6H_{12}Br_2Cl_2N_4$
Formula weight	370.92
Temperature/K	170.0(1)
Crystal system	Monoclinic
Space group	$P2_1/c$
a/Å	6.0091(12)
b/Å	14.422(3)
c/Å	13.655(3)
α/°	90
β/°	92.17(3)
γ/°	90
Volume/Å³	1182.5(4)
Z	4
$\rho_{calc}g/cm^3$	2.083
μ/mm^{-1}	7.277
F(000)	720.0
Crystal size/mm³	0.22 × 0.16 × 0.13
Radiation	MoKα (λ = 0.71073)
2Θ range for data collection/°	4.11 to 50.496
Index ranges	$-7 \le h \le 7, -17 \le k \le 17, -16 \le l \le 16$
Reflections collected	7988
Independent reflections	2144 [R_{int} = 0.0406, R_{sigma} = 0.0429]
Data/restraints/parameters	2144/0/127
Goodness-of-fit on F²	1.037
Final R indexes [I>=2σ (I)]	R_1 = 0.0296, wR_2 = 0.0649
Final R indexes [all data]	R_1 = 0.0413, wR_2 = 0.0694
Largest diff. peak/hole / e Å⁻³	0.59/-0.36

Table 13 - Crystal data and structure refinement for (HMTA) 2(ICl).

Empirical formula	$C_6H_{12}Cl_2I_2N_4$
Formula weight	464.90
Temperature/K	170.0(1)
Crystal system	Monoclinic
Space group	$P2_1/c$
a/Å	5.9773(12)
b/Å	15.148(3)
c/Å	14.032(3)
α/°	90
β/°	91.91(3)
γ/°	90
Volume/Å³	1269.9(4)
Z	4
ρ_{calc} *g/cm³*	2.432
μ/mm⁻¹	5.346
F(000)	864.0
Crystal size/mm³	0.2 × 0.15 × 0.13
Radiation	MoKα (λ = 0.71073)
2Θ range for data collection/°	3.958 to 57.706
Index ranges	-8 ≤ h ≤ 8, -19 ≤ k ≤ 20, -18 ≤ l ≤ 18
Reflections collected	10708
Independent reflections	3293 [R_{int} = 0.0385, R_{sigma} = 0.0421]
Data/restraints/parameters	3293/0/127
Goodness-of-fit on F²	1.038
Final R indexes [I>=2σ (I)]	R_1 = 0.0278, wR_2 = 0.0513
Final R indexes [all data]	R_1 = 0.0354, wR_2 = 0.0534
Largest diff. peak/hole / e Å⁻³	0.55/-0.76

Table 14 - Crystal data and structure refinement for (HMTA) 2(NBP).

Empirical formula	$C_{11}H_{12}BrN_3O_2$
Formula weight	298.15
Temperature/K	293(2)
Crystal system	Orthorhombic
Space group	$Pmn2_1$
a/Å	31.646(6)
b/Å	5.7998(7)
c/Å	5.9963(9)
α/°	90
β/°	90
γ/°	90
Volume/Å³	1100.5(3)
Z	4
$\rho_{calc}g/cm^3$	1.799
μ/mm^{-1}	3.728
F(000)	600.0
Crystal size/mm³	0.11 × 0.09 × 0.09
Radiation	MoKα (λ = 0.71073)
2Θ range for data collection/°	6.916 to 50.5
Index ranges	-37 ≤ h ≤ 37, -6 ≤ k ≤ 6, -7 ≤ l ≤ 7
Reflections collected	12123
Independent reflections	2012 [R_{int} = 0.1167, R_{sigma} = 0.0944]
Data/restraints/parameters	2012/1/154
Goodness-of-fit on F²	0.981
Final R indexes [I>=2σ (I)]	R_1 = 0.0501, wR_2 = 0.0618
Final R indexes [all data]	R_1 = 0.0680, wR_2 = 0.0669
Largest diff. peak/hole / e Å⁻³	0.49/-0.70
Flack parameter	-0.007(15)

Table 15 - Crystal data and structure refinement for (HMTA) 2(NBS).

Empirical formula	$C_{29}H_{41}Br_4Cl_3N_{12}O_8$
Formula weight	1111.73
Temperature/K	170.0(1)
Crystal system	Triclinic
Space group	*P*-1
a/Å	6.7019(13)
b/Å	7.1733(14)
c/Å	21.591(4)
α/°	98.26(3)
β/°	96.45(3)
γ/°	99.19(3)
Volume/Å³	1004.3(4)
Z	1
ρ_{calc} *g/cm³*	1.838
μ/mm⁻¹	4.271
F(000)	554.0
Crystal size/mm³	0.11 × 0.09 × 0.08
Radiation	MoKα (λ = 0.71073)
2Θ range for data collection/°	5.776 to 50.498
Index ranges	-8 ≤ h ≤ 6, -8 ≤ k ≤ 8, -25 ≤ l ≤ 23
Reflections collected	6946
Independent reflections	3602 [R_{int} = 0.0299, R_{sigma} = 0.0474]
Data/restraints/parameters	3602/0/271
Goodness-of-fit on F²	1.139
Final R indexes [I>=2σ (I)]	R_1 = 0.0417, wR_2 = 0.0957
Final R indexes [all data]	R_1 = 0.0522, wR_2 = 0.0995
Largest diff. peak/hole / e Å⁻³	0.55/-0.43

Table 16 - Crystal data and structure refinement for (HMTA)•4(NBS) @CH_2Cl_2.

Empirical formula	$C_{42}H_{56}Br_7Cl_4N_{15}O_{14}$
Formula weight	1696.18
Temperature/K	170.0(1)
Crystal system	Triclinic
Space group	*P*-1
a/Å	7.4375(15)
b/Å	12.392(3)
c/Å	17.214(3)
α/°	102.13(3)
β/°	94.58(3)
γ/°	103.14(3)
Volume/Å^3	1496.9(6)
Z	1
ρ_{calc}g/cm^3	1.882
μ/mm^{-1}	4.942
F(000)	838.0
Crystal size/mm^3	0.13 × 0.11 × 0.09
Radiation	MoKα (λ = 0.71073)
2Θ range for data collection/°	3.472 to 50.498
Index ranges	-7 ≤ h ≤ 8, -14 ≤ k ≤ 14, -20 ≤ l ≤ 19
Reflections collected	11370
Independent reflections	5387 [R_{int} = 0.0792, R_{sigma} = 0.1561]
Data/restraints/parameters	5387/36/391
Goodness-of-fit on F^2	1.026
Final R indexes [I>=2σ (I)]	R_1 = 0.0710, wR_2 = 0.1261
Final R indexes [all data]	R_1 = 0.1457, wR_2 = 0.1516
Largest diff. peak/hole / e Å^{-3}	0.79/-0.75

Table 17 - Crystal data and structure refinement for (HMTA) 4(NBS)@CCl_4.

Empirical formula	$C_{24}H_{28}Br_4Cl_{10}N_8O_8$
Formula weight	1230.68
Temperature/K	170.0(1)
Crystal system	Tetragonal
Space group	$P4_2/nmc$
a/Å	17.682(3)
b/Å	17.682(3)
c/Å	7.2014(14)
α/°	90
β/°	90
γ/°	90
Volume/Å^3	2251.5(8)
Z	2
ρ_{calc}g/cm^3	1.815
μ/mm^{-1}	4.218
F(000)	1204.0
Crystal size/mm^3	0.16 × 0.14 × 0.1
Radiation	MoKα (λ = 0.71073)
2Θ range for data collection/°	6.108 to 57.756
Index ranges	-24 ≤ h ≤ 23, -24 ≤ k ≤ 23, -9 ≤ l ≤ 9
Reflections collected	20226
Independent reflections	1567 [R_{int} = 0.0647, R_{sigma} = 0.0317]
Data/restraints/parameters	1567/0/105
Goodness-of-fit on F^2	1.051
Final R indexes [I>=2σ (I)]	R_1 = 0.0358, wR_2 = 0.0860
Final R indexes [all data]	R_1 = 0.0577, wR_2 = 0.0949
Largest diff. peak/hole / e Å^{-3}	0.60/-0.55

Table 18 - Crystal data and structure refinement for (HMTA) 2(NIS).

Empirical formula	$C_{14}H_{20}I_2N_6O_4$
Formula weight	590.16
Temperature/K	120.0(1)
Crystal system	Monoclinic
Space group	*P*2/*c*
a/Å	7.3937(3)
b/Å	7.0761(3)
c/Å	18.4375(9)
α/°	90
β/°	93.580(4)
γ/°	90
Volume/Å³	962.74(7)
Z	2
ρ_{calc}*g/cm³*	2.036
μ/mm⁻¹	3.299
F(000)	568.0
Crystal size/mm³	0.189 × 0.127 × 0.041
Radiation	MoKα (λ = 0.71073)
2Θ range for data collection/°	5.758 to 50.498
Index ranges	-8 ≤ h ≤ 7, -8 ≤ k ≤ 4, -11 ≤ l ≤ 22
Reflections collected	3188
Independent reflections	1738 [R_{int} = 0.0411, R_{sigma} = 0.0723]
Data/restraints/parameters	1738/0/119
Goodness-of-fit on F²	1.250
Final R indexes [I>=2σ (I)]	R_1 = 0.0541, wR_2 = 0.1292
Final R indexes [all data]	R_1 = 0.0677, wR_2 = 0.1364
Largest diff. peak/hole / e Å⁻³	2.11/-0.99

Table 19 - Crystal data and structure refinement for (HMTA) 4(NIS)@CH_2Cl_2.

Empirical formula	$C_{26}H_{36}Cl_8I_4N_8O_8$
Formula weight	1379.83
Temperature/K	170.0(1)
Crystal system	Tetragonal
Space group	$P4_2/nmc$
a/Å	17.299(2)
b/Å	17.299(2)
c/Å	7.8162(16)
α/°	90
β/°	90
γ/°	90
Volume/Å³	2339.1(8)
Z	2
$\rho_{calc}g/cm^3$	1.959
μ/mm^{-1}	3.171
F(000)	1320.0
Crystal size/mm³	0.13 × 0.11 × 0.08
Radiation	MoKα (λ = 0.71073)
2Θ range for data collection/°	4.71 to 50.474
Index ranges	-20 ≤ h ≤ 20, -20 ≤ k ≤ 20, -8 ≤ l ≤ 9
Reflections collected	14655
Independent reflections	1131 [R_{int} = 0.1571, R_{sigma} = 0.0765]
Data/restraints/parameters	1131/0/78
Goodness-of-fit on F²	1.148
Final R indexes [I>=2σ (I)]	R_1 = 0.0746, wR_2 = 0.0887
Final R indexes [all data]	R_1 = 0.1289, wR_2 = 0.0998
Largest diff. peak/hole / e Å⁻³	0.60/-0.61

Cofinanciado por:

SUOMEN TASAVALLAN

REPUBLIC OF FINLAND

UNIÃO EUROPEIA

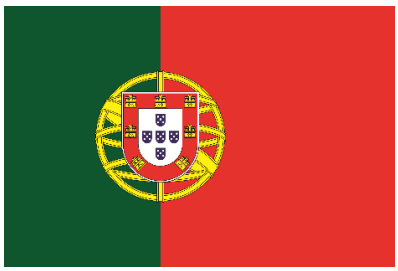

GOVERNO DA REPÚBLICA PORTUGUESA

REGIÃO AUTÓNOMA DA MADEIRA